A Holistic Approach to Reactivity-Controlled Compression Ignition Engine Performance: 4E Analysis (Evaporation, Energy, Emissions, Exergy) and Multidimensional Efficiency Metrics under Varying Engine Speed

Mehran Nazemian[1*], Mehrdad Nazemian[2]

[1]Lecturer in the Mechanical Department, Vahdat institute of Higher Education, Torbat-e Jam

[2]Master's degree graduate, Mechanical Engineering, Sahand University of Technology, Tabriz

ARTICLE INFO	A B S T R A C T
	This study investigates the performance of Reactivity-Controlled Compression Ignition (RCCI) engines under varying engine speeds using a 4E approach (Evaporation, Energy, Emissions, Exergy) and introduces innovative multidimensional efficiency indices. A 1.9-liter TDI Volkswagen engine was modeled in CONVERGE CFD software to analyze spray dynamics, combustion processes, and emissions across different engine speeds. New indices, including Evaporation-Energy Performance Index (EvEPI), Emission-Energy Synergy Index (EmESI), and Exergy-Emission Balance Index (ExEmBI), were developed to evaluate engine performance comprehensively. Results reveal that optimal performance occurs within 1600–2200 RPM, where fuel evaporation, combustion efficiency, and exergy utilization are maximized while emissions are minimized. For instance, at 3100 RPM, EvEPI increases sharply to 9857.17 mg/ms, reflecting enhanced evaporation but also highlighting risks of non-uniform fuel-air mixing at high speeds. Conversely, EmESI for HC rises from 33.04 gr/kW.h at 1000 RPM to 284.90 gr/kW.h at 3100 RPM, indicating increased unburned hydrocarbons due to incomplete combustion. NOx emissions decrease from 11.51 gr/kW.h at 1600 RPM to 2.28 gr/kW.h at 3100 RPM, aligning with reduced combustion temperatures. Higher speeds lead to elevated HC and CO emissions due to shorter mixing times, while lower speeds increase NOx due to prolonged combustion durations. Exergy analysis shows total and second-law efficiencies peak at lower speeds, emphasizing the importance of optimizing operational parameters. These findings provide valuable insights for designing efficient, low-emission RCCI engines.

1.Introduction

Internal combustion engines (ICEs) have long been a cornerstone of modern transportation and industrial applications. However, with the growing concerns over environmental pollution, climate change, and public health, there has been an increasing emphasis on improving the efficiency and reducing the emissions of these engines. In recent years, researchers and engineers have focused on addressing the challenges associated with compression ignition (CI) engines, particularly in terms of enhancing

*Corresponding Author
Email Address: Mehran_nazemian@yahoo.com
https://doi.org/10.22068/ase.2025.700

combustion efficiency and mitigating harmful emissions such as particulate matter and nitrogen oxides (NOx) [1].

To optimize environmental and economic costs, research efforts have been directed toward simultaneously reducing emissions while maintaining high engine efficiency. This has led to the development of advanced combustion strategies based on low-temperature combustion (LTC) that do not require catalytic aftertreatment systems. These advanced strategies typically focus on controlling the start of combustion to improve fuel-air mixing, which results in a reduction in local equivalence ratio, temperature, or both [2], thereby categorizing them as LTC strategies. One such strategy is Reactivity Controlled Compression Ignition (RCCI), which offers high thermal efficiency while significantly reducing NOx and soot emissions. In RCCI engines, a low-reactivity fuel is premixed with air and introduced into the combustion chamber through the intake port, while a high-reactivity fuel is directly injected into the combustion chamber. This fuel delivery approach enables better control over the combustion phase, pressure rise rate, and heat release rate (HRR) [3].

A wide range of studies has been conducted on RCCI engines with various research objectives. One of the primary challenges identified in RCCI combustion is the relatively higher levels of unburned hydrocarbons (HC) and carbon monoxide (CO) emissions compared to conventional spark-ignition (SI) and CI engines. A key research focus within RCCI engine development is optimizing combustion chamber geometry. Studies have demonstrated that piston bowl depth has a significant impact on gross indicated efficiency (GIE) and heat transfer characteristics [4-7].

Fuel injection parameters also play a critical role in the performance and emissions of RCCI engines. For example, selecting an appropriate spray angle along with reducing injection pressure has been shown to lower HC and CO emissions while enhancing GIE [8, 9]. Other studies have examined early diesel injection timing, which resulted in reduced CO and unburned hydrocarbons (UHC) but an increase

in NOx emissions [10-12]. This phenomenon occurs due to the transition from mixture-controlled to reaction-controlled combustion [13].

Another parameter that has been investigated by researchers on RCCI engines is the nozzle hole diameter (NHD). Nazemian et al. [14] examined the effect of nozzle hole diameter (NHD) in an RCCI engine using CFD simulations. Reducing the NHD to 130 µm decreased the Sauter Mean Diameter (SMD) to 15.49 µm and increased the number of droplets by 24%, leading to improved evaporation, fuel-air mixing, and faster combustion. However, excessively reducing the NHD resulted in increased NOx emissions, while using a larger NHD (175 µm) led to the formation of larger droplets and reduced combustion efficiency. The optimal NHD range (150-160 µm) provided maximum combustion efficiency (92.04%) and net indicated efficiency (38.58%). These results highlight the critical role of optimized NHD in enhancing engine performance and reducing emissions.

Another crucial parameter affecting RCCI engine performance and emissions is exhaust gas recirculation (EGR). Several studies have highlighted the necessity of EGR, particularly at higher engine speeds, to optimize RCCI engine operation [3]. Research has shown that increasing the EGR rate reduces peak pressure rise rate, NOx emissions, and soot formation [15-18]. This reduction is primarily attributed to the thermal and dilution effects of EGR, which lower the in-cylinder temperature. However, some studies have reported that increasing EGR levels leads to higher UHC and CO emissions due to the formation of locally fuel-rich regions [15, 18].

Despite extensive research on RCCI engine performance and emissions, most studies have focused on fuel injection parameters, while the influence of operational parameters, such as engine speed, has received comparatively less attention.

Several studies have investigated the effect of engine speed on RCCI engine performance and emissions. Asad et al. [19] conducted an experimental study analyzing the impact of

A Holistic Approach to Reactivity-Controlled Compression Ignition Engine Performance: 4E Analysis (Evaporation, Energy, Emissions, Exergy) and Multidimensional Efficiency Metrics under Varying Engine Speed

engine speed under LTC conditions on emissions such as NOx and soot. Their results indicated that prolonged mixing time and oxygen availability in the fuel contribute to reduced NOx and soot emissions. Paykani et al. [20] examined the effect of increasing engine speed and found that reduced residence time for chemical reactions led to more incomplete combustion, lower peak pressure and temperature, and delayed combustion phasing. Additionally, CO and UHC emissions increased to unacceptable levels. Benajes et al. [21] concluded that high CO and UHC emissions persisted across all engine speeds due to crevice volume effects. Dahodwala et al. [22] demonstrated that the injection timing at which combustion behavior changes occurs earlier with increasing engine speed. Their findings also showed that NOx emissions were higher at lower engine speeds, while THC and CO emissions were lower. Hanson et al. [23] reported that increasing engine speed led to reduced NOx emissions but higher soot and CO emissions. Wang et al. [24]observed that NOx emissions increased at lower engine speeds. Finally, Splitter et al. [4] found that higher engine speeds resulted in reduced NOx emissions.

On the other hand, in recent years, engine designers have concluded that the efficiency derived from the first law alone often does not provide a clear understanding of the operational mechanisms of an internal combustion engine. Rakopoulos et al. [25] were the first to investigate exergy variations in internal combustion engines. In their study, a diesel engine was simulated using a single-zone thermodynamic model, and the changes in different exergy terms were analyzed during the compression, combustion, and expansion processes. Subsequent studies expanded on this approach by conducting exergy analyses in gasoline and diesel engines. These studies examined exergy variations during various engine processes and assessed the influence of different parameters on exergy flow in internal combustion engines [26, 27]. Uçkan et al. [28] investigated the second-law analysis of a dual-fuel engine operating with methanol and diesel.

Their study demonstrated that exergy efficiency is significantly influenced by fuel composition and injection strategies. The authors emphasized the importance of optimizing fuel reactivity to minimize exergy destruction during combustion. Proniewicz et al. [29] evaluated the energy and exergy performance of a diesel engine operating with diesel, biodiesel, and ammonia. Their findings indicated that ammonia could serve as a viable alternative fuel, achieving comparable thermal and exergy efficiency while reducing greenhouse gas emissions. Singh et al. [30] conducted a comprehensive performance analysis of a diesel engine fueled with blends of waste cooking oil and pyrolyzed polyethylene oil. Their study highlighted the significance of exergy stability indices and demonstrated that these blends could substantially enhance engine performance while mitigating environmental impacts.

Exergy analysis of low-temperature combustion was investigated by Amjad et al. [31], who analyzed exergy variations within the combustion chamber of an HCCI engine fueled with a natural gas and n-heptane blend. Several other studies also examined exergy analysis for low-temperature combustion, evaluating the effects of various operating parameters on different exergy terms during the combustion process [32, 33]. Khaliq et al. [34-36]conducted an exergy analysis of an HCCI engine operating with ethanol and hydrogen. The thermodynamic model used in their study incorporated a global chemical kinetic mechanism. However, given that low-temperature combustion is highly dependent on fuel chemistry, the results of their study provided limited insights into chemical exergy.

Further research has focused on assessing the impact of various parameters on the exergy performance of RCCI engines. Li et al. [37] analyzed the first- and second-law efficiencies for three combustion regimes: conventional diesel combustion, homogeneous charge compression ignition (HCCI), and reactivity-controlled compression ignition (RCCI). Their study revealed that in-cylinder temperature, equivalence ratio during combustion, combustion temperature, chemical reactivity

A Holistic Approach to Reactivity-Controlled Compression Ignition Engine Performance: 4E Analysis (Evaporation, Energy, Emissions, Exergy) and Multidimensional Efficiency Metrics under Varying Engine Speed

reactivity fuel in an RCCI engine. Their findings showed that optimizing the premixed ratio of acetylene and diesel significantly improved combustion and exergy efficiency while reducing emissions. This study highlighted the potential of acetylene as an alternative fuel for enhancing RCCI engine performance. Baodong Ma et al. [49] conducted an exergy analysis of a dual-fuel diesel-methanol engine. Their study demonstrated that adjusting the methanol energy fraction and utilizing high-pressure EGR could substantially reduce exergy losses, improve combustion efficiency, and ensure compliance with stringent emissions regulations. Kumar et al. [50] evaluated the performance and emissions of a hydrogen-biodiesel dual-fuel engine under Reactivity Controlled Compression Ignition (RCCI) conditions. The results of this study indicate that the introduction of hydrogen enhances combustion efficiency and reduces exergy destruction, consequently leading to a reduction in emissions of unburned hydrocarbons and particulate matter. Feng et al. [51] investigated the combustion characteristics of methanol-diesel blends with co-solvents. Exergy analysis revealed that blending methanol with diesel improves combustion efficiency and reduces exergy losses, although it may result in increased NOx emissions. Taghavifar et al. [52] assessed the performance of an RCCI engine fueled with diesel and hydrogen. The results of this research indicated that increasing the compressor pressure ratio and optimizing combustion duration can improve exergy efficiency and reduce irreversibility.

Recent studies have focused on integrating advanced thermodynamic, economic, and environmental assessments to improve the sustainability of RCCI engines. Doğan et al. [53] conducted a comprehensive exergoeconomic and exergoenvironmental analysis of an RCCI engine fueled by n-heptane and isopropanol blends, incorporating Life Cycle Assessment (LCA). Their findings highlight that increasing intake air temperature (IAT) reduces exergy destruction and improves exergy efficiency. Additionally, the study linked thermodynamic performance to economic viability, showing that higher IAT leads to lower power generation

costs. The exergoenvironmental analysis, based on ISO 14040 standards, revealed that increasing fuel amounts amplified the environmental impact of exergy losses. Their holistic approach to sustainability sets this study apart from conventional research focusing solely on performance or emissions. Similarly, Asgari et al. [54] explored co-generation in an RCCI engine using solar steam reforming of methanol to produce syngas as the low-reactivity fuel. Their multi-objective optimization approach combined exergy, thermoeconomic, and exergoenvironmental analyses. Key findings include an exergy efficiency of 38.14%, with SCO_2 turbine inlet temperature as a crucial parameter. The High-Temperature Recuperator (HTR) and RCCI engine were identified as major sources of exergy destruction. The study also evaluated economic feasibility, incorporating unit product cost (UPC), net present value (NPV), and payback period (PP) under different pricing scenarios. Their MOPSO-based optimization ensured an optimal trade-off between exergy and economic performance.

Although several studies have explored 3E, 4E, and 5E analyses, comprehensive research that integrates multiple E factors simultaneously in internal combustion engines (ICEs) remains relatively scarce. For instance, Bayramoğlu et al. [55] conducted an analysis of energy, exergy, and emissions (3E) in a dual-fuel compression ignition (CI) engine fueled with hydrogen-enriched B20 biodiesel-diesel blends. Their findings indicated that B20 increased CO_2 emissions, while hydrogen addition reduced them, owing to its carbon-free nature. Moreover, they observed that fuel consumption and exhaust energy increased with load, whereas exergy destruction decreased. Notably, B20 exhibited the lowest energy and exergy efficiencies due to its lower calorific value and higher viscosity, which hindered overall system performance.

In a similar vein, Saravanan et al. [56] performed an investigation on energy, exergy, entropy, emission factors, and sustainability index (4E) in a single-cylinder diesel engine using thermally cracked waste paraffin

oil and di-ethyl ether-diesel blends. Among the tested blends, BSS60 demonstrated the highest energy (28.50%) and exergy (30.35%) efficiencies, the lowest entropy generation, and the highest sustainability index. Additionally, BSS60 reduced CO emissions, though it led to a 3.37% increase in NOx emissions compared to pure diesel. These results underscore the potential trade-offs in fuel blend optimization, where a reduction in one emission may inadvertently lead to an increase in another.

Building on these findings, Manickam et al. [57] expanded the analysis to encompass the 5E attributes, including combustion, performance, emissions, exergy, and economic aspects, in a CI engine fueled with a 25% papaya seed oil-diesel blend (P25), along with hydrogen and diethyl ether (DEE) additions. The study revealed that hydrogen premixing (6–10 LPM) enhanced brake thermal efficiency (BTE), reduced brake-specific fuel consumption (BSFC), and improved both exergy efficiency and the sustainability index. In contrast, DEE addition (10–20%) resulted in decreased BTE, exergy efficiency, and the sustainability index. Furthermore, hydrogen increased in-cylinder pressure and heat release rate, while significantly reducing CO_2 emissions. However, DEE exhibited mixed effects on emissions, as it lowered combustion intensity and showed less favorable outcomes for NOx and CO emissions. These observations further highlight the complex interplay between fuel additives and engine performance in multi-fuel CI engine configurations.

This study aims to comprehensively assess the impact of engine speed variation on thermodynamic performance, exergy, emissions, and the evaporation process in an RCCI engine. In this context, new indices have been developed to evaluate engine performance under varying operational conditions, and the relationships between these indices have been analyzed. The necessity of this study arises from the absence of a comprehensive framework for evaluating RCCI engine performance under the influence of engine speed changes. While previous studies have primarily focused on the effects of injection parameters and fuel composition, the broader impact of engine speed (RPM) on

overall RCCI engine performance has been less thoroughly explored. Moreover, this research represents the first attempt to simultaneously investigate fuel evaporation, energy, exergy, and emissions across a wide range of engine speeds.

A key motivation for this study is to identify a representative operational point of the engine. Selecting the appropriate engine speed can directly influence energy efficiency, emissions reduction, and exergy performance. Thus, this study aims to identify an engine speed range that strikes a suitable balance among these parameters. Additionally, this research addresses challenges related to RCCI combustion at both low and high engine speeds. At low speeds, incomplete combustion and prolonged combustion duration can result in lower efficiency, while at high speeds, although fuel evaporation improves, shorter fuel and air residence times in the cylinder may lead to reduced energy efficiency and increased pollutants such as HC and CO. Therefore, this study aims to provide solutions to mitigate these challenges and optimize engine performance across various operational conditions.

The primary impetus for this study is the need to develop new indices for more accurate engine performance analysis. Traditional indices, such as thermodynamic efficiency, are insufficient to fully characterize engine performance. To address this, new indices, including EvEPI, EmESI, ExEmBI, and EvEmII, have been introduced to facilitate a more detailed analysis of evaporation, energy, exergy, and emissions parameters. These indices contribute to a deeper understanding of the complex interactions between variables influencing engine performance and provide a foundation for the design and optimization of RCCI engines.

1. Problem description and methodology

The engine modeled in this study was a 1.9-liter TDI Volkswagen light-duty engine, which was purchased from the Advanced Power Systems Research Center at the University of Michigan. The VW TDI engine is a 4-cylinder diesel engine equipped with a variable-geometry turbocharger, and its specifications are provided

A Holistic Approach to Reactivity-Controlled Compression Ignition Engine Performance: 4E Analysis (Evaporation, Energy, Emissions, Exergy) and Multidimensional Efficiency Metrics under Varying Engine Speed

in Table 1. For n-heptane fuel injection into each cylinder, CRDI injectors (described in Table 2) were employed.

Table 1: Features of the engine available at the Advanced Power Systems Research Center at the University of Michigan used in this study.

Parameter	Value
Cylinder arrangement	Inline 4
Cylinder bore/stroke (mm)	79.5/95.5
Geometric Compression ratio	17:1
IVC (aTDC)	-169
EVO (aTDC)	162
Piston bowl	Mexican hat
Max. Power (kW)	66 @ 3750 RPM
Max. Torque (Nm)	210 @ 1900 RPM

Table 2: Specifications of the Bosch direct-injection injector for the used engine.

Injector Type	CRDI
Number of holes	6
Nozzle diameter (mm)	0. 165
Included spray angle (°)	144
Injection pressure (bar)	400

In this study, the three-dimensional computational fluid dynamics (CFD) simulation software CONVERGE was employed to model all processes within the RCCI engine from the IVC moment as the intake valve was closed in the chamber teemed with premixed air-methane gas to the EVO moment when the exhaust valve opened to release pollutants. Hence, the n-heptane fuel injection process, including

atomization, breakups, and coalescence, was modeled to predict the quality and quantity of fuel droplets in interaction with the air-methane gas. The evaporated and combusted droplets were modeled through a kinetic mechanism comprising 76 species and 464 reactions [58]. The thermodynamic characteristics of the formed species were simulated by solving the continuity, Navier-Stokes, energy, turbulence, and chemical kinetics equations for each computational cell in the temporal domain. The Droplet distinct Model (DDM) [59] was used to simulate the injection process. For spray breakup, the Modified KH-RT models [60, 61] were used. The first breakup occurs when the high-pressure fuel jet initially disintegrates into larger droplets as it exits the injector nozzle, driven by instabilities and interactions with the surrounding premixed air-methane. The second breakup occurs as larger droplets are further fragmented into finer droplets due to aerodynamic forces during their travel through the combustion chamber. Both stages are crucial for achieving a fine fuel mist, which enhances mixing with air, leading to more efficient combustion, better fuel efficiency, and reduced emissions. The applied turbulence model is the RNG k-ε model [62], while the heat transfer process is simulated using the Wall function model of Han and Reitz [62]. The NTC model [60] was used to simulate collisions, with post-collision outcomes [63] further analyzed using the collision outcome model. The interaction between droplets and walls was modeled using the Wall film model [64], and to speed up the runtime, a Multi-zone chemistry solver [65] is implemented. To enhance the geometric accuracy inside the cylinder, a three-dimensional scan is used to model the cylinder chamber, considering the injector locations. The meshing process in the Converge CFD software is performed automatically using the Adaptive Mesh Refinement (AMR) method to enhance the computational accuracy during code execution. A 360° meshing was employed due to the off-center nature of the piston bowl, as shown in Figure 1. The default size of the computational cells was set to 5 mm, resulting in a mesh network of 150,000 cells.

Figure 1: Mesh configuration of combustion chamber.

In this study, the engine speed was varied to assess its effects on spray characteristics, including droplet size and distribution within the combustion chamber, as well as performance parameters such as heat transfer, combustion efficiency, and gross indicated efficiency (GIE). Additionally, pollutant emissions, including HC, CO, and NOx, and various exergy components were analyzed.

The analytical sequence of Evaporation, Energy, Emission, and Exergy was systematically and comprehensively designed to provide an in-depth understanding of the dynamic processes within the RCCI engine. This sequence was deliberately structured to reflect the natural progression of operational processes, from fuel spray dynamics to energy utilization and efficiency evaluation. The rationale behind this order is as follows:

I. Evaporation Analysis: Evaporation is positioned at the beginning of the study due to its critical role in the early stages of fuel injection and spray formation. Understanding the evaporation process is crucial as it directly influences combustion quality and heat transfer within the cylinder. Spray dynamics, including injection pressure, injection velocity, droplet size distribution, and fuel atomization, significantly impact subsequent combustion processes. Therefore, evaluating evaporation first allows for a more effective and comprehensive examination of how fuel behavior influences energy production and pollutant formation, ensuring a logical progression in the analysis.

II. Energy Analysis: Following evaporation, the focus shifts to energy analysis, which includes key parameters such as ignition delay, combustion duration, in-cylinder pressure, temperature, and heat release rate (HRR). Energy production and its efficiency are central to assessing engine performance. This analysis is crucial for evaluating fundamental performance criteria, such as thermal efficiency and combustion efficiency. Since energy generation directly influences pollutant formation, it is essential to examine energy parameters first to better understand their relationship with emissions.

III. Emission Analysis: Emission analysis follows energy evaluation, serving as a critical step in understanding the environmental impact of the engine. The formation of pollutants, including HC, CO, and NOx, is heavily influenced by combustion efficiency and energy production within the engine. Given the direct correlation between pollutant formation and combustion processes, placing emissions analysis after energy assessment ensures a logical approach. This sequence facilitates a detailed examination of how operational and injection parameters affect emissions and provide a comprehensive evaluation of the engine's environmental and operational performance.

IV. Exergy Analysis: Finally, exergy analysis is conducted to assess the thermodynamic efficiency of the engine and quantify system inefficiencies. Exergy analysis provides deeper insights into energy losses and inefficiencies, which are essential for optimization. Positioning exergy analysis at the end of the study aligns with its role in evaluating overall system efficiency, following the assessment of energy production and emissions. This analysis offers valuable insights into fuel utilization and waste heat recovery, concluding the study with an evaluation of the engine's thermodynamic performance and overall sustainability.

This structured analytical approach, progressing from Evaporation to Energy, then to Emissions, and finally to Exergy, ensures a systematic and comprehensive understanding of the complex processes

A Holistic Approach to Reactivity-Controlled Compression Ignition Engine Performance: 4E Analysis (Evaporation, Energy, Emissions, Exergy) and Multidimensional Efficiency Metrics under Varying Engine Speed

governing RCCI engine performance. Each analysis builds upon the previous one, creating a logical and coherent flow from the fuel injection stage to the final evaluation of energy efficiency and environmental impact. This methodology not only facilitates a holistic evaluation but also emphasizes the interactions between fuel dynamics, combustion performance, emissions, and energy efficiency, which are crucial for optimizing engine performance and minimizing environmental impact in RCCI engines.

Finally, based on the computed results and output data from CONVERGE software, innovative indices have been developed to establish a comprehensive analytical framework for evaluating the impact of engine speed variations on evaporation (spray dynamics), energy, emissions, and exergy. These indices precisely characterize the interrelationships between fuel evaporation, energy efficiency, exergy, emissions, and other relevant variables, providing a novel perspective for a deeper understanding of RCCI engine behavior under varying operating conditions.

2. Governing equations

3.1. Conservation relationships

To predict the behavior of fuels and products in fluid and gaseous phases, the required continuity, momentum, energy, and chemical kinetics equations are written as follows [66]:

$$\frac{\partial \rho}{\partial t} + \frac{\partial \rho u_i}{\partial x_i} = S \tag{1}$$

$$\frac{\partial \rho u_i}{\partial t} + \frac{\partial \rho u_i u_j}{\partial x_j} = -\frac{\partial P}{\partial x_i} + \rho g_i + \frac{\partial \sigma_{ij}}{\partial x_j} + S_i \tag{2}$$

$$\frac{\partial \rho e}{\partial t} + \frac{\partial u_j \rho e}{\partial x_j} = -P \frac{\partial u_j}{\partial x_j} + \sigma_{ij} \frac{\partial u_i}{\partial x_j} + \frac{\partial}{\partial x_j}\left(K \frac{\partial T}{\partial x_j}\right) + \frac{\partial}{\partial x_j}(\rho D \sum_m h_m \frac{\partial Y_m}{\partial x_j}) + S \tag{3}$$

$$\frac{\partial \rho_m}{\partial t} + \frac{\partial \rho_m u_j}{\partial x_j} = \frac{\partial}{\partial x_j}\left(\rho D \frac{\partial Y_m}{\partial x_j}\right) + S_m \tag{4}$$

where the symbols represent the following physical quantities: u denotes velocity, ρ stands for density, S represents the source term for thermal energy, P is pressure, Y_m indicates the mass fraction of species m, D is the diffusivity coefficient, e is the specific internal energy, K denotes thermal conductivity, h_m is the specific enthalpy, σ_{ij} is the stress tensor, and T represents temperature.

3.2. The relationship between spray dynamics

In this investigation, a Lagrangian drop Eulerian fluid approach was adopted to model the spray dynamics, where the liquid phase was treated as a dispersed phase with physical attributes corresponding to diesel fuel derived from the CONVERGE fluid property library (Tetradecane) [6-8, 67-69]. These attributes, such as vapor pressure, density, specific heat capacity, and surface tension, can be parameterized as functions of temperature. The modeling of fine droplets in the spray employs a statistical framework using Lagrangian particles termed parcels, which represent ensembles of droplets with similar size characteristics. The Blob injection strategy is implemented in which parcels are stochastically initialized within the nozzle hole with an initial radius equivalent to the nozzle radius, delineating the primary core of the liquid spray. The initialized parcels serve as parent entities constituting the entirety of the liquid spray core. To represent droplet breakup phenomena, a modified Kelvin-Helmholtz-Rayleigh-Taylor (KH-RT) model is employed, comprising distinct stages of primary and secondary breakup [61]. The KH instability model was applied to predict the primary breakup of the injected fuel parcels, while the secondary breakup mechanism, which was attributable to aerodynamic instabilities, was captured through the RT instability model. A schematic depiction of the KH-RT model breakup time is provided in equation 5:

$$\tau_{KH} = \frac{3.726 B_1 R}{\Omega_{KH} \Lambda_{KH}} \tag{5}$$

Where B_1 is an adjustable parameter, and Ω_{KH} and Λ_{KH} represent the frequency and wavelength calculated for the mode with the fastest growth. As evident from Eq. (5), smaller values of B_1 lead to faster breakup, resulting in a higher degree of mixing in the spray process.

The radius of the resulting daughter droplet is calculated as follows:

$$r_c = \frac{\pi C_{RT}}{K_{RT}} \tag{6}$$

Where K_{RT} is the calculated wave number and C_{RT} is an adjustable parameter, typically set to a value of 0.1. This parameter significantly influences the distribution of fuel vapor in the cylinder. The smaller values of C_{RT} result in the production of smaller droplets, leading to their rapid evaporation and consequently contributing to the generation of a higher premixed content.

3.3. Energy relationships

The gross indicated efficiency is calculated from the produced work (W_{gross}) and power (P_{gross}) as follows [68, 69].

$$W_{gross}\left[\frac{kJ}{cycle}\right] = \int_{-180}^{+180} P dV \tag{7}$$

$$P_{gross}[kW] = W_{gross} \times Engine\ Speed[rpm]/120 \tag{8}$$

$$GIE\ (\%) = \frac{W_{gross}}{\dot{m}_{n-heptane} \times LHV_{n-heptane} + \dot{m}_{methane} \times LHV_{methane}} \times 100 \tag{9}$$

where the lower heating value of heptane fuel is 42.3 MJ/kg, whereas that of methane fuel is 50 MJ/kg [70, 71].

The combustion efficiency is also assessed as follows [72]:

$$\eta_c = \frac{\sum HRR}{\dot{m}_{n-heptane} \times LHV_{n-heptane} + \dot{m}_{methane} \times} \times 100 \tag{10}$$

Where, $\sum HRR$ is the cumulative heat release rate.

The following relationship represents the emission [73]:

$$Emission\ (\frac{gr}{kWh}) = \frac{\dot{m}_{emission}}{Power_{gross}} \tag{11}$$

The combustion start and duration are respectively measured as follows [74, 75]:

Combustion duration = CA90 - CA50

Starting point of combustion = CA10

Where CA10, CA50, and CA90 represent the crank angles at which 10%, 50%, and 90% of the fuel is combusted.

The mixing Time is calculated using the following equation [21]:

$$Mixing\ Time = CA10 - End\ of\ injection \tag{12}$$

3.4. Exergy relationships

The exergy refers to the maximum producible work of a system, provided that during a reversible process, the system reaches thermal and mechanical equilibrium with the surroundings while only exchanging heat with the environment [7, 33, 76, 77]. In general, the exergy balance of a closed system is performed using Equation (13). The exergy loss due to heat transfer is calculated using Equation (14). In this equation, T represents the average temperature of the mixture inside the combustion chamber, while T_0 denotes the ambient temperature. The amount of heat loss is obtained by solving the governing equations.

$$\frac{dA}{d\theta} = \frac{dA_w}{d\theta} - \frac{dA_q}{d\theta} - \frac{dI}{d\theta} + \frac{dA_{ch}}{d\theta} \tag{13}$$

A Holistic Approach to Reactivity-Controlled Compression Ignition Engine Performance: 4E Analysis (Evaporation, Energy, Emissions, Exergy) and Multidimensional Efficiency Metrics under Varying Engine Speed

$$\frac{dA_q}{d\theta} = \left(1 - \frac{T_0}{T}\right)\frac{dQ}{d\theta} \tag{14}$$

Equation (15) is used to calculate work exergy, where P is the pressure inside the combustion chamber, and P_0 is the ambient pressure. Work exergy equals the net work performed, which is determined by the difference between the work done on the system and the work done on the surroundings [7, 33, 76, 77].

$$\frac{dA_w}{d\theta} = (P - P_0)\frac{dV}{d\theta} \tag{15}$$

Equation (16) is applied to calculate the changes in the chemical exergy of the mixture inside the combustion chamber. The variation in the chemical exergy of the mixture consists of the sum of the changes in the chemical exergy of methane fuel and the changes in the exergy of diesel fuel. The chemical exergy changes of other species are neglected due to their negligible values [7, 33, 76, 77]. $a_{f,CH4}$ and $a_{f,diesel}$ represent the chemical exergy of methane and diesel fuels, respectively. The chemical exergy of a fuel corresponds to the maximum work generated from the fuel's combustion and its complete conversion into combustion products, including carbon dioxide and water. The employed equations are presented in detail in the following [7, 33, 76, 77]:

$$\frac{dA_{ch}}{d\theta} = \left(\frac{dm_{CH4}}{d\theta} \times a_{fv,CH4}\right) \tag{16}$$
$$+ \left(\frac{dm_{C_7H_{16}}}{d\theta} \times a_{fv,C_7H_{16}}\right)$$

$$a_{fv} = a_{fv,thermomechanical} + a_{fv,chemical} \tag{17}$$

$$a_{fv,thermomechanical} = h_{fv} - T_0 s_{fv} - g_{fv}^0 \tag{18}$$

$$
\begin{aligned}
a_{fv,chemical} &= g_{fv}^0 - \alpha g_{CO2}^0 \\
&- \left(\frac{\beta}{2}\right)g_{H2O}^0 \left(\alpha + \frac{\beta}{4} - \frac{\gamma}{2}\right)g_{O2}^0 \\
&- RT_0\ln\left(\frac{\alpha^\alpha \left(\frac{\beta}{2}\right)^{\frac{\beta}{2}} \varepsilon^\varepsilon}{\zeta^\zeta \left(\alpha + \frac{\beta}{4} - \frac{\gamma}{2}\right)^{\alpha + \frac{\beta}{4} - \frac{\gamma}{2}}}\right)
\end{aligned}
\tag{19}
$$

$$\varepsilon = \frac{\left(\alpha + \frac{\beta}{4} - \frac{\gamma}{2}\right)}{0.21} \tag{20}$$

$$\zeta = 0.79\varepsilon + \alpha + \frac{\beta}{2} \tag{21}$$

The total exergy of a system consists of thermomechanical and chemical components. The thermomechanical exergy represents the maximum useful work obtainable as the system transitions to the ambient conditions ($T_0 = 298$ K and $P_0 = 1$ atm), a state known as the restricted dead state. This component is calculated using the following expression:

$$A_{tm} = (U - U^0) + P_0(V - V^0) - T_0(S - S^0) \tag{22}$$

The dead state is the condition where the system is in equilibrium with its environment. If only thermal and mechanical equilibrium is present while chemical equilibrium is not the system is considered to be in a restricted dead state, where its chemical composition remains unchanged. This assumption simplifies chemical exergy analysis in engineering applications [7, 33].

The second law of thermodynamics, for a closed cycle, is stated as below [7, 33, 76, 77]:

$$\eta_s = \frac{W}{(A_{ch} + A_{tm})_{IVC} + A_{ch,C7H16}} \tag{23}$$

3.5. Combined Relationships relationships

In this study, a novel set of composite indices is introduced for the first time, aiming to establish a comprehensive framework for analyzing the effects of engine speed variations on the performance of RCCI engines. These indices characterize the relationships between fuel evaporation, energy efficiency, exergy, emissions, and the interactions among these variables.

Traditional methods for evaluating engine performance primarily focus on thermal efficiency and emissions. However, these composite indices go beyond these conventional metrics by enabling a multidimensional analysis of the combustion process, energy conversion, and pollutant formation. This analytical framework holds significant potential for optimizing next-generation internal combustion engines. In the following sections, the definitions of the indices and their corresponding mathematical relationships are presented.

3.5.1. Evaporation-Energy Performance Index (EvEPI)

Since the fuel evaporation process directly influences combustion quality, energy release rate, and energy efficiency, the Evaporation-Energy Performance Index (EvEPI) has been developed to evaluate the relationship between fuel evaporation quality and the energy efficiency of RCCI engines. In previous studies, the relationship between evaporation and energy efficiency has been examined only qualitatively. However, this index enables a quantitative analysis of this relationship. The EvEPI is calculated using the following equation:

$$\text{EvEPI} \left[\frac{mg}{ms}\right] = \frac{\text{Effective Evaporation}}{GIE} \tag{24}$$

$$\text{Effective Evaporation} \left[\frac{mg}{ms}\right] = \left(\frac{\text{spray mass } [kg]}{SMD \, [m]} \times V_{injection} \left[\frac{m}{s}\right]\right) \times 1000 \tag{25}$$

Where spray mass, SMD (Sauter Mean Diameter), and $V_{injection}$ (injection velocity) represent the mass of the spray, the average droplet diameter, and the injection velocity, respectively. These three parameters are derived from CONVERGE CFD simulations and are used to determine the trend of this index under various engine operating conditions. Additionally, the EvEPI index is applied to investigate the effects of variations in SMD and $V_{injection}$ on energy efficiency and to identify optimal conditions for enhancing fuel evaporation and reducing energy consumption.

3.5.2. Emission-Energy Synergy Index (EmESI)

This index illustrates how the level of pollutants produced by the engine is influenced by energy efficiency. Higher values of this index indicate an increase in pollutant emissions relative to energy efficiency, and it is calculated as follows:

$$\text{EmESI}_i \left[\frac{gr}{kW.h}\right] = \frac{\text{Emission Level }_i}{GIE}, \qquad i \in HC, CO, NOx \tag{26}$$

Furthermore, the Emissions-Energy Synergy Index (EmESI) is used to analyze the impact of the synergy ratio between emissions and energy efficiency at different engine speeds, as well as to evaluate the increase or decrease in pollutant emissions during energy optimization.

3.5.3. Exergy-Emission Balance Index (ExEmBI)

This index represents the relationship between the engine's output exergy and the level of pollutants produced. A higher value of this index indicates greater exergy efficiency and reduced pollutant emissions. Consequently, this index is used to evaluate the ratio of output exergy to pollutant emissions and to determine optimal operating conditions. The Exergy-Emissions Balance Index (ExEmBI) is calculated as follows:

$$ExEmBI_i \left[\frac{kW.h}{gr}\right] = \frac{\text{Exergy Output}}{Emission\ Level_i}, \quad i \in HC, CO, NOx \quad (27)$$

3.5.4. Evaporation-Emission Interaction Index (EvEmII)

This index represents the extent to which the effective evaporation process contributes to the reduction of pollutant emissions. A higher value of this index indicates a greater role of fuel evaporation in reducing emissions. The index is calculated as follows:

$$EvEmII\ [kW] = \frac{\text{Effective Evaporation}}{Emission\ Level_i}, \quad i \in HC, CO, NOx \quad (28)$$

The primary application of this index is to determine the role of the evaporation process in reducing HC, CO, and NOx emissions. Additionally, it is used to evaluate injection and mixing conditions that enhance the evaporation rate and reduce pollutant emissions.

3.5.5. Exergy-Energy Utilization Index (ExEUI)

This index evaluates the ratio of output exergy to energy efficiency and quantifies the exergy utilization rate. A higher value of this index indicates more optimal utilization of exergy in the process of generating mechanical and thermal energy. The index is calculated as follows:

$$ExEUI\ [kW.h] = \frac{\text{Exergy Output}}{GIE} \quad (29)$$

The primary application of this index is to analyze the contribution of exergy to improving the overall efficiency of the engine and to investigate the effects of operational parameter variations on the optimal utilization of exergy in the engine.

3.5.6. Emission-Exergy Synergy Index (EmExSI)

This index represents the impact of exergy efficiency on pollutant emissions. A lower value of this index indicates that reducing exergy losses leads to lower emissions. The EmExSI is calculated using the following equation:

$$EmExSI_i \left[\frac{gr}{kW.h}\right] = \frac{Emission\ Level_i}{\eta_s}, \quad i \in HC, CO, NOx \quad (30)$$

The primary application of this index is to analyze the effect of exergy variations on emissions and to compare different pollutants under various exergy efficiency conditions.

3.5.7. Evaporation-Exergy Performance Index (EvExPI)

This index examines the relationship between effective fuel evaporation and exergy efficiency. A higher value of this index signifies the positive impact of fuel evaporation on optimal exergy utilization and combustion improvement. The EvExPI is determined using the following equation:

$$EvExPI\left[\frac{mg}{ms}\right] = \frac{\text{Effective Evaporation}}{\eta_s} \quad (31)$$

The EvExPI index is particularly useful for analyzing the correlation between evaporation quality and exergy, as well as for identifying optimal fuel injection conditions to enhance exergy efficiency.

3. Results and discussion

4.1. Validation

To validate the proposed CFD model, experimental results obtained from the laboratory of Michigan Technological University's engine facility were used. For the validation of the simulation results, two different operating conditions of the engine were

considered, as outlined in Table 3. The engine speed, BMEP (brake mean effective pressure), fuel injection strategy, and EGR level employed in these two operational modes are distinct from each other [8].

Figure 2 illustrates the prediction of the cylinder pressure and heat release rate by the simulation compared with the experimental values for the operational conditions presented in Table 3, showing good agreement with the measured cylinder pressure values. Additionally, Table 4 presents the predicted pollutants and their comparisons with the experimental values. Note that all simulations conducted in this study were based on case (a).

Table 3: Two operating conditions under which the light duty RCCI engine was simulated to validate the employed model.

Parameters	Case a	Case b
Speed (RPM)	1300	1500
BMEP (Bar)	4	5
Diesel flow rate (gr/s)	0.071	0.107
NG flow rate (gr/s)	0.5	0.56
Air flow rate (Kg/h)	60.736	55.95
SOI1/SOI2 (bTDC)	Singles - 20	55/20
Split type (%/%)	Single	70/30
T_IVC (K)	380	378
Common Rail Pressure (bar)	400	400
BR %	89	85
EGR%	0%	20%

Table 4: Validation of the employed model by comparing the simulation results of emissions for the two examined cases with those of the experiment.

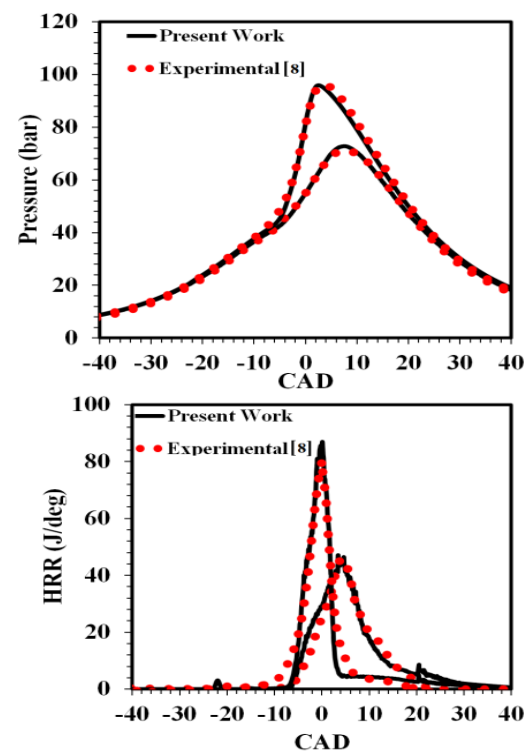| Emission	Case a		Case b	
	Exp	Sim	Exp	Sim
NOx (ppm)	860	723	670	1728
HC (ppm)	7800	4165	5300	3314
CO (ppm)	1380	673	1100	563

Figure 2: Validation of the in-cylinder pressure and HRR in cases (a) and (b)

4.2. Results

4.2.1. Evaporation Analysis

The effect of engine speed variation on fuel injection velocity and pressure is illustrated in Figure 3. Engine speed significantly impacts fuel injection characteristics. As the engine speed increases, the duration of each combustion cycle decreases, necessitating a higher fuel supply within a shorter timeframe. Consequently, both

Figure 3: Effect of engine speed on injection pressure and velocity.

injection pressure and velocity must increase to ensure adequate fuel supply and promote efficient atomization and combustion within the chamber.

Figure 4 presents the droplet size distribution and variations in the Sauter Mean Diameter (SMD) of fuel droplets across different engine speeds. The droplet size distribution clearly indicates that at higher engine speeds, due to elevated injection pressure and velocity, the fuel droplet size decreases. This occurs because higher pressure enhances fuel atomization, leading to finer droplets. Conversely, at lower engine speeds, the required fuel delivery per cycle decreases, leading to reduced injection pressure and velocity. These changes result in larger fuel droplets, as the lower injection force produces coarser atomization.

Additionally, the SMD profile shows that at the start of injection (20° before top dead center, BTDC), the fuel droplet size is equivalent to the injector nozzle diameter, i.e., 165 µm. As the crank angle advances to 19° and 18° BTDC, the fuel droplet size decreases due to the dominance of aerodynamic forces over surface tension. However, between 18° and 6° BTDC, the ongoing compression process increases momentum forces and turbulence within the combustion chamber, leading to droplet collisions and the formation of larger droplets.

Figure 5 illustrates the effect of engine speed on flow velocity and turbulent kinetic energy (TKE). The velocity distribution curve demonstrates that as the engine speed increases from 1000 RPM to 3100 RPM, the piston velocity, air flow velocity, and the velocity of the air-fuel mixture within the cylinder rise accordingly. These changes intensify turbulence inside the combustion chamber, leading to stronger vortex structures. The increase in airflow velocity and turbulence intensity directly contributes to higher TKE, as depicted in the figure [78].

Figure 4: Effect of engine speed on SMD and fuel droplet diameter.

This increase in TKE applies greater momentum forces on fuel droplets. If these forces surpass the surface tension of the droplets, droplet breakup accelerates, resulting in a decrease in fuel droplet size. Conversely, at lower engine speeds, reduced airflow velocity and weaker turbulence decrease TKE. Under such conditions, the lower momentum forces fail to overcome surface tension, leading to incomplete droplet breakup and larger fuel droplets. These larger droplets hinder fuel-air mixing quality, contributing to incomplete combustion, which may negatively impact engine performance and increase pollutant formation.
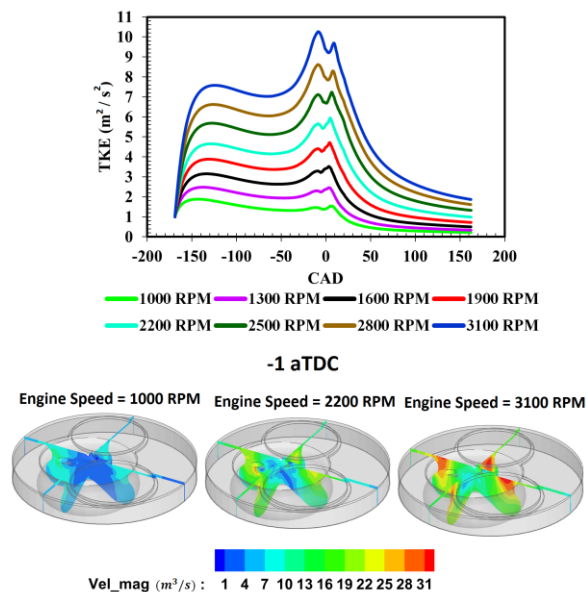

Figure 5: Effect of engine speed on TKE and Flow Velocity Magnitude.

Figure 6 presents the temperature distribution, droplet distribution, and fuel droplet size at 1000 RPM, 2200 RPM, and 3100 RPM. In general, smaller fuel droplets are advantageous in combustion, as their higher surface-area-to-volume ratio increases contact with surrounding air, enhancing fuel evaporation and chemical reaction rates. However, this advantage is contingent on adequate time and temperature for complete chemical reactions.

Figure 6: Droplet size distribution and Combustion temperature contours for different engine speed 1000 RPM, 2200 RPM and 3100 RPM

The results in this figure indicate that at 3100 RPM, despite smaller fuel droplet sizes, temperature distribution within the combustion chamber is non-uniform. This non-uniformity prevents complete fuel combustion throughout the chamber. In contrast, at 1000 RPM, fuel droplets maintain an optimal size, and temperature distribution is more uniform, facilitating complete combustion.

4.2.2. Energy Analysis

To further analyze the impact of engine speed on combustion efficiency and Gross Indicated Efficiency (GIE), Figure 7 is presented. The

findings indicate that engine speed variation significantly affects these parameters.

At lower engine speeds, combustion efficiency and GIE improve considerably due to the longer combustion cycle duration. The extended duration allows sufficient time for complete fuel-air mixing and evaporation, enabling thorough chemical reactions such as fuel decomposition and oxidation [20, 79]. As a result, combustion becomes more uniform and complete, leading to a gradual increase in cylinder pressure and temperature, ultimately enhancing combustion efficiency and GIE.

Conversely, at higher engine speeds, the combustion cycle duration shortens, reducing the time available for complete fuel evaporation and mixing. This limitation results in incomplete combustion, leading to a decline in GIE. The reduced cycle duration also causes a drop in cylinder pressure and temperature, decreasing the heat transfer duration between hot gases and cylinder walls. This further contributes to GIE reduction.

Additionally, at higher engine speeds, increased injection pressure and velocity improve fuel atomization, reducing droplet size. However, due to the limited combustion time, this improvement in atomization cannot fully compensate for the decreased combustion quality and GIE.

Figure 7: GIE and combustion efficiency at various engine speeds.

4.2.3. Emission Analysis

Figure 8 illustrates the impact of engine speed variation on HC, CO, and NOx emissions. The results indicate that engine speed significantly influences HC and CO formation.
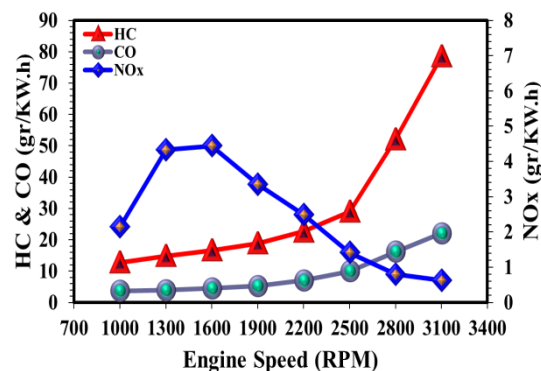

Figure 8: Pollutant HC, CO, and NOx produced for different engine speed.

At lower engine speeds, longer combustion cycles facilitate more complete combustion and improved fuel-air mixing, reducing HC and CO emissions [20, 22, 80]. The extended duration allows for complete fuel evaporation and complete chemical reactions. In contrast, at higher engine speeds, the shorter combustion duration leads to incomplete combustion, increasing HC and CO emissions. The reduction in cylinder pressure and temperature, along with limited fuel evaporation and mixing time, further contributes to increased pollutant formation, even though improved fuel atomization at higher injection pressures aids in better mixing. These findings highlight the necessity of optimizing engine speed to balance performance and emissions, emphasizing the critical role of combustion timing and mixing quality in minimizing HC and CO emissions.

In this section, the influence of engine speed on NOx emissions is examined. Previous studies suggest that variations in operational, geometric, and injection system parameters in internal combustion engines can lead to nonlinear behavior in performance and emissions [81]. Similarly, Figure 8 shows that engine speed variation induces a nonlinear trend in NOx emissions.

A Holistic Approach to Reactivity-Controlled Compression Ignition Engine Performance: 4E Analysis (Evaporation, Energy, Emissions, Exergy) and Multidimensional Efficiency Metrics under Varying Engine Speed

Figure 10: Temperature and thermomechanical exergy variation with respect to CAD and EVO for different engine speeds.

Since internal energy and entropy are temperature-dependent, thermomechanical exergy also follows a temperature-dependent pattern. As a result, the highest thermomechanical exergy occurs at lower engine speeds, whereas the lowest thermomechanical exergy is observed at higher engine speeds.

Figure 11 depicts the effect of varying engine speed on the cumulative heat release (CHR) and chemical exergy. At lower engine speeds, the slower piston movement results in a longer combustion cycle, allowing for extended fuel-air mixing and fuel evaporation. Additionally, more time is available for combustion reactions,
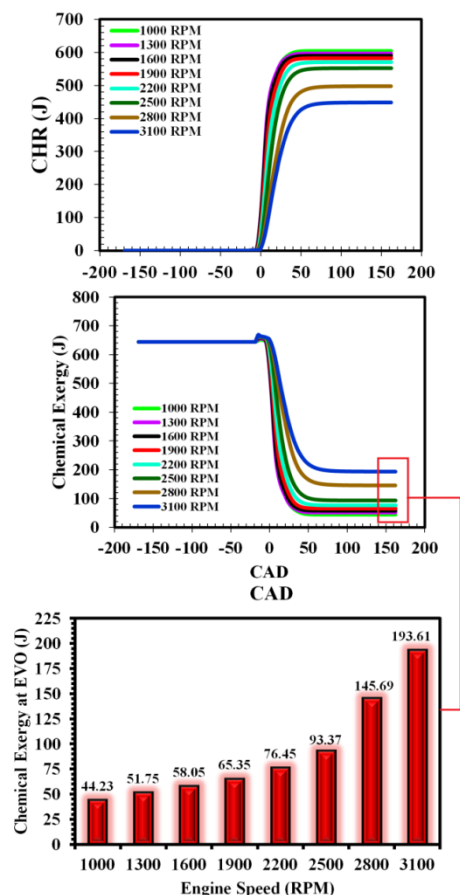
Figure 11: CHR and chemical exergy variation with respect to CAD and EVO for different engine speed.

including fuel decomposition and oxidation. As a result, CHR reaches its maximum at lower engine speeds and its minimum at higher engine speeds, confirming that incomplete combustion is more pronounced at higher speeds.

Chemical exergy is closely linked to CHR, as it represents the available energy in the fuel that can be converted into useful work. Consequently, chemical exergy is minimized at lower engine speeds and maximized at higher speeds.

Figure 12 illustrates work exergy at various engine speeds. The highest work exergy is observed at exhaust valve opening (EVO) for engine speeds ranging from 1000 to 1600 RPM, while the lowest work exergy is recorded at 3100 RPM. According to the CHR trend, more cumulative energy is released at lower engine

4722   Automotive Science and Engineering (ASE)

speeds, leading to higher work output. Therefore, operating at lower engine speeds results in increased work exergy.

Figure 13 displays the heat transfer and heat transfer exergy at different engine speeds. As shown, at lower engine speeds, the combustion cycle duration increases, allowing for more heat transfer from the combustion gases to the cylinder walls. This extended contact time between the hot gases and the cylinder walls enhances heat transfer, leading to an increase in heat transfer exergy at lower engine speeds. It can be concluded that heat transfer is a function of engine speed, with maximum heat transfer exergy occurring at the lowest engine speed and minimum heat transfer exergy recorded at 3100 RPM.

Figure 13: Heat transfer and Heat transfer exergy variation with respect to CAD and EVO for different engine speed.

Figure 14 presents the variation of irreversibility at different crank angles and at EVO under various engine speeds. As observed, during combustion, significant chemical reactions increase entropy production, causing a considerable rise in irreversibility.

Although it was expected that lower in-cylinder temperatures and reduced heat transfer at higher engine speeds would result in lower irreversibility at EVO, this phenomenon was not observed. The primary reason for increased irreversibility at high engine speeds can be inferred from Figure 8, which depicts the influence of engine speed on pollutant emissions (HC, CO, and NOx).

Figure 12: Work exergy variation with respect to CAD and EVO for different engine speed.

reactions. Conversely, at higher speeds, reduced combustion time results in incomplete combustion, increasing HC and CO emissions. The lower cylinder pressure and temperature further contribute to higher pollutant formation due to insufficient mixing and evaporation time.

Regarding NOx emissions at lower engine speeds, the prolonged combustion cycle allows for extended fuel-air mixing and fuel evaporation, resulting in a gradual increase in in-cylinder temperature and pressure. Since NOx formation is highly temperature-dependent and occurs predominantly above 1500°C, its production is maximized at lower speeds due to higher combustion temperatures and pressures.

In the analysis of internal combustion engine performance, two key metrics for evaluating energy efficiency and system irreversibility are the total exergy efficiency and the second law efficiency. These metrics provide insights into how effectively the fuel's energy is utilized while accounting for thermodynamic constraints.

Factors influencing total exergy efficiency include heat losses, incomplete combustion, and heat transfer. Similarly, second law efficiency is affected by incomplete combustion, which leads to the production of CO and HC, increasing system irreversibility, as well as heat losses.

Figure 15 presents the variations in total exergy efficiency and second law efficiency across different engine speeds. These plots indicate that both efficiencies decrease with increasing engine speed and improve at lower speeds. This trend highlights that more complete combustion at lower speeds enhances overall efficiency and performance, emphasizing its significance in engine design and optimization.

Figure 14: Irreversibility variation with respect to CAD and EVO for different engine speed.

At higher engine speeds, the in-cylinder temperature is lower compared to lower speeds. Lower combustion temperatures lead to incomplete combustion, resulting in higher emissions of CO and HC. These unburned fuel species possess lower energy content than CO2 and H2O, thereby reducing the efficiency of chemical energy conversion and increasing entropy production. The presence of these emissions not only leads to higher energy losses but also enhances system irreversibility.

Overall, Figure 8 indicates that engine speed significantly affects the production of HC and CO. At lower speeds, longer combustion cycles promote more complete combustion and improved fuel-air mixing, leading to lower HC and CO emissions. The extended combustion duration allows for complete fuel evaporation and proper chemical

Figure 15: Total exergy efficiency and second law efficiency at various engine speeds.

4.2.5. Index Combined Analysis

The Evaporation-Energy Performance Index (EvEPI) represents the ratio of effective fuel evaporation to gross indicated efficiency (GIE) and serves as a crucial metric for assessing the impact of fuel injection and evaporation processes on the engine's energy efficiency. A higher EvEPI indicates enhanced fuel evaporation and its more effective contribution to the combustion process.

As shown in Figure 16, EvEPI increases sharply with rising engine speed, escalating from 517.98 mg/ms at 1000 RPM to 9857.17 mg/ms at 3100 RPM. This substantial rise is attributed to the reduction in Sauter Mean Diameter (SMD) and the increased injection velocity at higher engine speeds (see Figure 4).

At low engine speeds (1000–1300 RPM), the index remains low due to the lower injection velocity and pressure, which result in larger fuel droplets and reduced evaporation. Under these conditions, combustion duration is longer, and mixing quality improves, but the overall evaporation rate remains limited.

At medium engine speeds (1600–2200 RPM), EvEPI experiences a significant increase, indicating improved fuel evaporation and enhanced air-fuel mixing rates. This trend is primarily due to the reduction in SMD caused by the higher injection pressure and velocity (see Figure 4).

At high engine speeds (2500–3100 RPM), EvEPI rises steeply, reaching its peak value of 9857.17 mg/ms. This trend is mainly

driven by the further reduction in droplet diameter and the acceleration of evaporation due to increased turbulent kinetic energy (TKE) and in-cylinder fluid motion.

However, an excessive increase in this index at high speeds is not necessarily desirable, as an overly high evaporation rate may lead to non-uniform fuel-air mixture distribution, negatively impacting combustion quality.
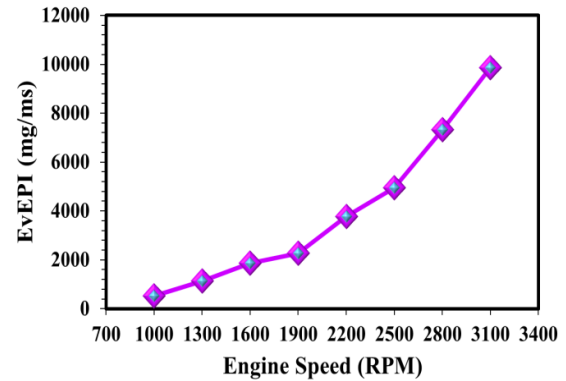
Figure 16: EvEPI at various engine speeds.

In this section, the Emission-Energy Synergy Index (EmESI) is analyzed, as shown in Figure 17. This index evaluates the emissions of pollutants such as HC, CO, and NOx relative to the Gross Indicated Efficiency (GIE). A higher value of this index indicates an increase in pollutants per unit of energy produced, signifying a decrease in combustion quality and an increase in engine inefficiency. The index is calculated separately for each of the three pollutants (HC, CO, and NOx) to determine their individual impact on energy efficiency.
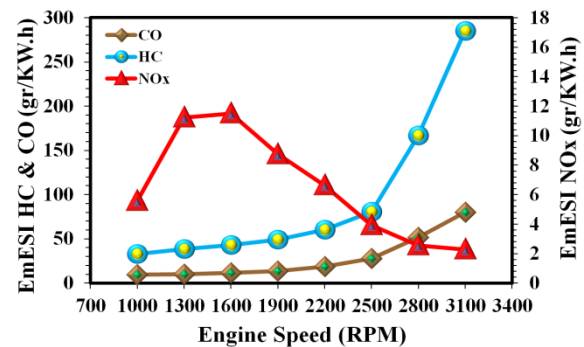
Figure 17: EmESI HC, CO and NOx at various engine speeds.

A Holistic Approach to Reactivity-Controlled Compression Ignition Engine Performance: 4E Analysis (Evaporation, Energy, Emissions, Exergy) and Multidimensional Efficiency Metrics under Varying Engine Speed

As shown in the figure, at low engine speeds (1000–1600 RPM), the $EmESI_{HC}$ value ranges from 33.04 to 43.20 gr/kW.h, indicating more complete combustion and a reduction in unburned hydrocarbons (HC). In this range, combustion time is longer, and the fuel-air mixture is more optimized.

At medium engine speeds (1900–2200 RPM), the index value increases and reaches 60.46 gr/kW.h at 2200 RPM, due to a relative reduction in combustion time and an increase in combustion chamber temperature.

At high engine speeds (2500–3100 RPM), $EmESI_{HC}$ increases sharply, reaching 284.90 gr/kW.h at 3100 RPM. This increase is primarily due to reduced mixing time and incomplete combustion in this range. Under these conditions, the fuel does not have enough time to mix and evaporate properly, leading to an increase in HC. This trend aligns with the increase in HC shown in Figure 8.

The changes in the EmESI index for CO emissions shown in this figure indicate that at low engine speeds (1000–1600 RPM), $EmESI_{CO}$ ranges from 9.57 to 11.61 gr/kW.h, indicating more complete combustion and lower concentrations of carbon monoxide (CO). At medium engine speeds (1900–2200 RPM), the value of the index increases but remains at a relatively controlled level.

At high engine speeds (2500–3100 RPM), $EmESI_{CO}$ increases sharply from 27.61 gr/kW.h at 2500 RPM to 80.14 gr/kW.h at 3100 RPM. This increase is due to reduced temperature and pressure in the cylinder, resulting in incomplete combustion and higher CO formation. This trend corresponds to the decline in combustion efficiency (shown in Figure 7) and the increase in CO (shown in Figure 8).

Additionally, the trend for the EmESI index for NOx emissions occurs non-linearly. As observed in the figure, the $EmESI_{NOx}$ value initially increases and then decreases, indicating a nonlinear dependence of NOx on temperature and combustion time. This trend is consistent

with the decrease in NOx shown in Figure 8 and the drop in temperature shown in Figure 10.

At low engine speeds (1000–1600 RPM), the value of this index increases from 5.55 to 11.51 gr/kW.h. This increase is due to higher temperature and pressure inside the combustion chamber and more complete combustion in this range.

At medium engine speeds (1900–2200 RPM), the index reaches its peak value of 11.51 gr/kW.h at 1600 RPM, which corresponds to the peak value of NOx in this range (as shown in Figure 8).

At high engine speeds (2500–3100 RPM), the $EmESI_{NOx}$ value decreases, reaching 2.28 gr/kW.h at 3100 RPM. This decrease is due to the lower temperature and pressure in the cylinder at high speeds, leading to fewer NOx formation reactions.

In Figure 18, the Exergy-Emission Balance Index (ExEmBI) is shown, which evaluates the output exergy relative to the emissions of HC, CO, and NOx. A higher value of this index indicates more optimal use of exergy and a reduction in emissions relative to useful energy produced. Conversely, a lower value indicates increased exergy waste and greater emissions relative to the exergy produced. This index is broken down into three components: $ExEmBI_{HC}$, $ExEmBI_{CO}$, and $ExEmBI_{NOx}$, each showing different trends with respect to changes in engine speed.

Figure 18: ExEmBI HC, CO and NOx at various engine speeds.

As the engine speed increases from 1000 to 3100 RPM, the value of $ExEmBI_{HC}$ decreases from 0.189 kW.h/gr to 0.043 kW.h/gr. This decreasing trend reflects the increased HC emissions at higher speeds, which is due to the reduced combustion time and poorer fuel-air mixing. At lower speeds (1000–1600 RPM), the index is relatively high, as the longer combustion cycle allows enough time for evaporation, mixing, and more complete combustion. However, with the increase in engine speed, the combustion time decreases, leading to incomplete combustion and increased HC emissions (as shown in Figure 8). As a result, the useful output exergy relative to HC emissions decreases, and the $ExEmBI_{HC}$ index drops.

The $ExEmBI_{CO}$ follows a similar trend to HC, decreasing from 0.655 kW.h/gr at 1000 RPM to 0.155 kW.h/gr at 3100 RPM. This significant decrease indicates that incomplete combustion worsens at higher speeds, leading to higher CO emissions. At lower speeds, the CO emissions are low compared to output exergy, as the temperature and pressure in the cylinder provide better conditions for complete combustion. However, at higher speeds, the reduced combustion time and increased piston speed lead to a shorter opportunity for the oxidation of CO into CO_2, causing CO levels to rise. This increase in CO leads to a further decrease in the $ExEmBI_{CO}$ index, suggesting that exergy waste in the form of unburned pollutants increases at higher engine speeds.

In contrast to HC and CO, the $ExEmBI_{NOx}$ index behaves differently. Initially, it decreases from 1.130 kW.h/gr at 1000 RPM to 1.005 kW.h/gr at 2200 RPM, but then increases sharply to 5.457 kW.h/gr at 3100 RPM. This nonlinear behavior is attributed to the effect of temperature on NOx formation. In the range from 1000 to 2200 RPM, increasing engine speed raises the cylinder temperature and pressure, creating conditions more favorable for NOx formation. Therefore, NOx emissions increase, and the ratio of NOx to output exergy increases, leading to a decrease in $ExEmBI_{NOx}$. However, at high speeds (2500–3100 RPM), the combustion time shortens and combustion temperature drops (as shown in Figure 10),

resulting in a decrease in NOx formation. On the other hand, the output exergy remains high, which causes the $ExEmBI_{NOx}$ index to rise. This increase indicates a reduction in NOx emissions at higher speeds, in contrast to the trends of HC and CO emissions.

Figure 19 presents the EvEmII index for three pollutants (HC, CO, and NOx). This index demonstrates how the rate of evaporation correlates with the reduction or increase in various emissions. A higher value indicates that an increase in evaporation rate is accompanied by a reduction in emissions, while a lower value suggests that an increase in evaporation has not reduced emissions and may have even led to higher emissions.
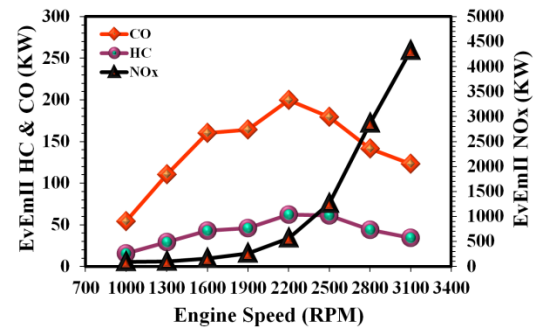
Figure 19: EvEmII HC, CO and NOx at various engine speeds.

For HC emissions, the EvEmII index increases from 15.67 kW at 1000 RPM to 29.23 kW at 1300 RPM. This increase indicates that the higher evaporation rate leads to a reduction in HC emissions, as more time is available for complete combustion in this range. In the intermediate RPM range (1600–2200 RPM), the index continues to rise and reaches 62.29 kW at 2200 RPM, reflecting an optimal balance between evaporation and HC reduction. However, at higher RPMs (2500–3100 RPM), the $EvEmII_{HC}$ value decreases, reaching 34.59 kW at 3100 RPM. This decrease is due to the increased HC production from incomplete combustion, as the shorter combustion cycle limits the complete burning of hydrocarbons (as shown in Figure 8).

The trend of the EvEmII index for CO follows a similar pattern to HC. At lower and intermediate RPMs (1000–2200 RPM), the

A Holistic Approach to Reactivity-Controlled Compression Ignition Engine Performance: 4E Analysis (Evaporation, Energy, Emissions, Exergy) and Multidimensional Efficiency Metrics under Varying Engine Speed

index increases because the higher evaporation improves combustion, resulting in lower CO emissions. However, at higher RPMs (2500–3100 RPM), the index decreases due to incomplete combustion, which increases CO levels caused by the relatively rich fuel-air mixture in some regions (as shown in Figure 8).

In contrast to HC and CO, the trend of the EvEmII index for NOx behaves differently. At lower speeds, the $EvEmII_{NOx}$ value is not high, as although evaporation is high, the combustion temperature is still not sufficient to produce significant NOx emissions. In the intermediate range (1600–2200 RPM), the index reaches its peak value, as the increased evaporation and optimized combustion lead to higher temperatures and enhanced NOx formation. Finally, at higher speeds (2500–3100 RPM), the index decreases, as reduced combustion time and lower temperatures result in lower NOx production.

Figure 20 displays the trend of the Exergy-Energy Utilization Index (ExEUI) at different engine speeds. This index represents the ratio of output exergy to energy efficiency, serving as a measure of how effectively the produced exergy is utilized in comparison to the input energy to the engine. The trend in Figure 20 shows that at lower speeds, the index remains almost constant, while at higher speeds, it increases.

From 1000 to 1900 RPM, the ExEUI is stable, ranging from 0.000436 to 0.000442 kW.h. This stability indicates an optimal balance between useful exergy and energy efficiency within this range. At these speeds, combustion is more efficient due to the longer cycle time, which allows more time for fuel evaporation and mixing. As a result, a larger portion of the chemical energy of the fuel is converted into useful work. This is confirmed by comparing the trend with Figure 11 (chemical exergy) and Figure 12 (work exergy), as in this range, chemical exergy is at its lowest, and most of it is converted into work exergy.

Figure 20: ExEUI at various engine speeds.

As the engine speed increases to the range of 2200 to 3100 RPM, the ExEUI shows an increasing trend, reaching 0.000618 kW.h at 3100 RPM. At first glance, this increase might suggest improved performance; however, further analysis of supplementary data reveals that this increase is mainly due to a rise in residual exergy in the cylinder and exhaust gases, rather than an increase in useful work. According to Figure 11, at higher speeds, the chemical exergy increases, indicating incomplete combustion and the presence of more unreacted fuel in the combustion chamber. Additionally, Figure 12 shows a decrease in work exergy at these speeds, which indicates a reduction in the engine's effective output power.

Furthermore, the changes in ExEUI should be examined in conjunction with the heat transfer trend (Figure 13) and irreversibility (Figure 14). At lower speeds, more exergy is transferred as heat to the cylinder walls, while at higher speeds, this amount decreases. This reduction in heat transfer could indicate increased energy retention within the combustion chamber, leading to higher localized temperature and pressure in certain areas, but it may also suggest uneven temperature distribution and reduced fuel-air mixing quality, which can negatively affect the overall engine performance. On the other hand, Figure 14 (irreversibility) shows an increase in irreversibility at higher speeds, meaning that a significant portion of the exergy is lost through thermodynamic inefficiencies rather than being converted into useful work. Therefore, the rise in ExEUI at higher engine speeds is more due to increased exergy loss and

incomplete combustion than to improved performance.

The results of this analysis indicate that the range of 1600 to 2200 RPM is the optimal performance range in terms of the balance between useful exergy and energy efficiency. Within this range, the maximum amount of useful work is extracted from the fuel, and the least exergy is wasted. In contrast, at higher speeds, the increase in ExEUI suggests increased fuel consumption without a corresponding increase in power production, which implies a reduction in the overall system efficiency. These findings emphasize the need for strategies to improve combustion conditions, reduce irreversibility, and increase the amount of extractable work exergy at higher engine speeds to prevent the undesirable increase in ExEUI.

The Emission-Exergy Synergy Index (EmExSI) is shown in Figure 21. This index represents the ratio of pollutant emissions (HC, CO, NOx) to exergy efficiency, indicating how much pollution is produced for each unit of useful exergy generated. A higher value of this index implies that, despite energy and exergy consumption, the engine continues to produce high levels of pollutants, reflecting a decrease in exergy efficiency and an increase in losses.

As shown in the figure, at low engine speeds (1000–1600 RPM), the value of $EmExSI_{HC}$ increases from 36.91 gr/kW.h at 1000 RPM to 48.27 gr/kW.h at 1600 RPM. Similarly, $EmExSI_{CO}$ rises from 10.69 gr/kW.h at 1000 RPM to 12.98 gr/kW.h at 1600 RPM, and $EmExSI_{NOx}$ increases from 6.20 gr/kW.h at 1000 RPM to 12.86 gr/kW.h at 1600 RPM. The reason for these results at lower engine speeds is the high amount of useful exergy produced, but the increase in NOx emissions is due to the elevated combustion chamber temperature. The combustion quality is good, but some HC and CO emissions remain due to incomplete combustion.
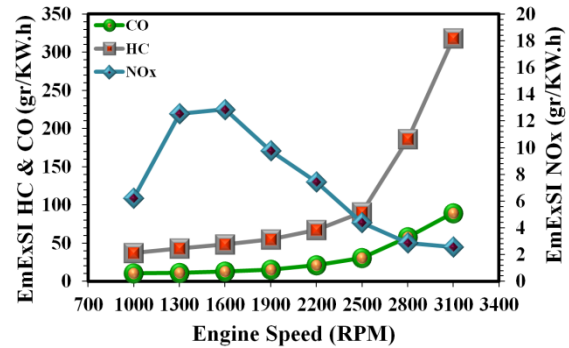
Figure 21: EmExSI HC, CO and NOx at various engine speeds.

At medium engine speeds (1900–2200 RPM), the $EmExSI_{HC}$ value increases to 55.11 gr/kW.h at 1900 RPM and then to 67.55 gr/kW.h at 2200 RPM. Additionally, $EmExSI_{CO}$ increases to 15.40 gr/kW.h at 1900 RPM and then to 21.08 gr/kW.h at 2200 RPM. However, $EmExSI_{NOx}$ initially decreases to 9.77 gr/kW.h at 1900 RPM and further reduces to 7.42 gr/kW.h at 2200 RPM. The trend in EmExSI for all three pollutants at medium speeds is due to the optimal combination of fuel evaporation and mixing, which reduces NOx. However, the increase in pressure and temperature leads to faster combustion, gradually increasing HC and CO emissions.

At high engine speeds (2500–3100 RPM), the $EmExSI_{HC}$ value sharply increases to 90.18 gr/kW.h at 2500 RPM and then to 318.30 gr/kW.h at 3100 RPM. $EmExSI_{CO}$ also shows a significant rise, from 30.84 gr/kW.h at 2500 RPM to 89.54 gr/kW.h at 3100 RPM. However, $EmExSI_{NOx}$ decreases from 4.39 gr/kW.h at 2500 RPM to 2.54 gr/kW.h at 3100 RPM. The reason for these results at high engine speeds is the significant degradation in combustion quality, resulting in the production of large amounts of HC and CO due to incomplete combustion (see Figure 8). Furthermore, as engine speed increases, the combustion cycle time shortens, and fuel does not have enough time for complete combustion. Finally, the reduction in combustion chamber temperature at high speeds causes a significant decrease in NOx production, as NOx is formed at temperatures above 1500K (see Figure 8).

Automotive Science and Engineering (ASE)   4729

A Holistic Approach to Reactivity-Controlled Compression Ignition Engine Performance: 4E Analysis (Evaporation, Energy, Emissions, Exergy) and Multidimensional Efficiency Metrics under Varying Engine Speed

Figure 22 illustrates the Evaporation-Exergy Performance Index (EvExPI), which represents the ratio of effective fuel evaporation to exergy efficiency. This index indicates how the rate of fuel evaporation changes relative to the engine's output exergy. Output exergy represents the amount of energy that can be converted into useful work, and an increase or decrease in this index provides valuable insights into the overall efficiency of the engine.
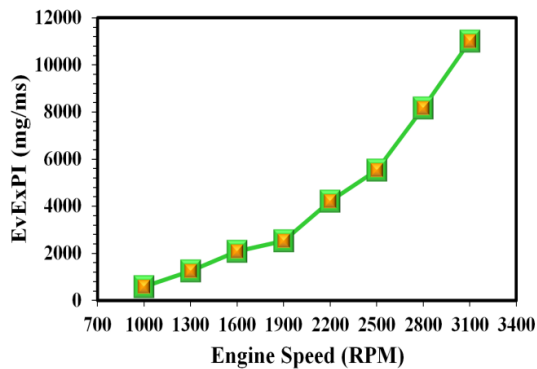

Figure 22: EvExPI at various engine speeds.

At low engine speeds (1000–1600 RPM), the EvExPI increases from 578.71 mg/ms at 1000 RPM to 2081.88 mg/ms at 1600 RPM. This rise is due to improved evaporation processes driven by longer combustion duration and better fuel-air mixing quality. In this range, the reduction in SMD (see Figure 4) and the increase in turbulent kinetic energy (TKE) (see Figure 5) contribute to better evaporation, while exergy efficiency remains at an acceptable level.

At medium engine speeds (1900–2200 RPM), the index continues to rise and reaches 4208.64 mg/ms at 2200 RPM. The increased injection pressure and velocity result in further reduction of SMD and an enhanced evaporation rate. The turbulence inside the cylinder facilitates better mixing and faster evaporation, keeping exergy efficiency high (see Figure 15). This range could be considered the optimal operational point for the engine from the perspective of this index, as it exhibits high evaporation rates while maintaining a good exergy efficiency.

At high engine speeds (2500–3100 RPM), EvExPI shows a sharp increase, reaching 11012.85 mg/ms at 3100 RPM. This significant increase is due to the rapid rise in evaporation rate compared to exergy efficiency. With the increased injection pressure and velocity, fuel droplets become smaller, and evaporation reaches its peak. However, at the same time, the engine's output exergy decreases. This decrease is caused by higher heat losses (see Figure 13) and increased irreversibility (see Figure 14), which reduce exergy efficiency. As a result, while evaporation increases, the overall engine performance does not improve, and there is a notable increase in exergy losses. Hence, an excessive increase in this index at higher speeds signals increased fuel consumption and decreased engine efficiency.

The trend of EvExPI closely resembles that of EvEPI (see Figure 16), as both indices emphasize evaporation rates. However, the key difference in EvExPI is that evaporation is measured relative to exergy, so at high speeds, the decrease in exergy efficiency leads to a sharp increase in the index. Additionally, this index has a close connection with the ExEUI index (see Figure 20), as the reduction in exergy efficiency at high speeds directly impacts the disproportionate growth of EvExPI. In this range, the reduced pressure and temperature inside the cylinder (see Figure 10) result in incomplete combustion, which leads to increased HC and CO emissions (see Figure 8), further affecting exergy efficiency.

The results of this analysis indicate that the 1600–2200 RPM range exhibits the best performance in terms of this index, as both evaporation rates are high and exergy efficiency remains at an optimal level. In contrast, at speeds above 2500 RPM, the sharp increase in EvExPI indicates high fuel consumption and reduced exergy efficiency, which can lead to decreased overall engine efficiency and increased energy losses.

4. Conclusion

This study provides a comprehensive analysis of the performance of Reactivity-Controlled Compression Ignition (RCCI) engines under varying engine speeds using a novel 4E approach (Evaporation, Energy, Emissions, Exergy) and introduces multidimensional efficiency indices to evaluate engine behavior. A 1.9-liter TDI Volkswagen engine was modeled in CONVERGE computational fluid dynamics (CFD) software to simulate spray dynamics, combustion processes, and emissions across a wide range of operating conditions. The research addresses critical challenges associated with RCCI combustion at both low and high engine speeds, offering valuable insights into optimizing operational parameters for improved energy efficiency, reduced emissions, and enhanced exergy performance.

Key findings from this study are summarized as follows:

Evaporation Analysis:

Engine speed significantly impacts fuel injection characteristics, including droplet size distribution and Sauter Mean Diameter (SMD). Higher engine speeds enhance fuel atomization, leading to smaller droplets and improved evaporation rates. However, excessively high speeds may result in non-uniform fuel-air mixing, negatively affecting combustion quality.

The Evaporation-Energy Performance Index (EvEPI) increases sharply with engine speed, reaching 9857.17 mg/ms at 3100 RPM, indicating enhanced fuel evaporation but highlighting the risks of incomplete combustion at high speeds.

Energy Analysis:

Combustion efficiency and gross indicated efficiency (GIE) improve at lower engine speeds due to longer combustion durations, allowing for better fuel-air mixing and more complete chemical reactions. Conversely, higher speeds reduce GIE due to shorter mixing times and incomplete combustion.

The optimal balance between energy efficiency and combustion quality occurs within the 1600–2200 RPM range, where fuel evaporation, combustion efficiency, and exergy utilization are maximized.

Emission Analysis:

NOx emissions exhibit a nonlinear trend, increasing at lower speeds due to elevated combustion temperatures and decreasing at higher speeds due to reduced temperatures and shorter combustion durations.

HC and CO emissions rise significantly at higher speeds due to incomplete combustion, with EmESI values for HC increasing from 33.04 gr/kW.h at 1000 RPM to 284.90 gr/kW.h at 3100 RPM.

The Exergy-Emission Balance Index (ExEmBI) highlights the trade-offs between output exergy and emissions, emphasizing the need for optimized operational conditions to minimize pollutant formation.

Exergy Analysis:

Total exergy efficiency and second-law efficiency decrease with increasing engine speed, underscoring the importance of optimizing combustion conditions to reduce irreversibility and improve thermodynamic performance.

Heat transfer exergy and irreversibility trends reveal that higher speeds lead to increased exergy losses, primarily due to incomplete combustion and elevated HC and CO emissions.

Multidimensional Efficiency Indices:

The introduced indices, including EvEPI, EmESI, ExEmBI, EvEmII, ExEUI, EmExSI, and EvExPI, provide a novel framework for evaluating the complex interactions between fuel evaporation, energy conversion, emissions, and exergy utilization. These indices facilitate a deeper understanding of RCCI engine behavior and offer practical guidance for optimizing engine performance.

The results of this study emphasize the importance of selecting an appropriate engine speed range to achieve optimal performance. The 1600–2200 RPM range emerges as the most favorable operational zone, balancing energy efficiency, emissions reduction, and exergy

A Holistic Approach to Reactivity-Controlled Compression Ignition Engine Performance: 4E Analysis (Evaporation, Energy, Emissions, Exergy) and Multidimensional Efficiency Metrics under Varying Engine Speed

performance. At higher speeds, while fuel evaporation improves, the shortened fuel and air residence times in the cylinder may lead to reduced energy efficiency and increased pollutants such as HC and CO. Conversely, at lower speeds, prolonged combustion durations and elevated in-cylinder temperatures result in higher NOx emissions. Therefore, this study provides solutions to mitigate these challenges and optimize engine performance across various operational conditions.

This research contributes to the development of advanced thermodynamic analyses and composite indices for internal combustion engines, providing a foundation for designing efficient, low-emission RCCI engines. Future studies should focus on integrating these findings with real-time control strategies and exploring the potential of alternative fuels to further enhance RCCI engine sustainability. Additionally, investigating the impact of external factors such as ambient temperature and altitude on engine performance could provide further insights. By addressing the challenges identified in this study, significant progress can be made toward achieving cleaner, more efficient combustion technologies for the transportation sector.

List of symbols

Nomenclature

t	Time (s)
u	Velocity (m/s)
S	Thermal energy source (W/Kg)
Y	Mass fraction
D	Diffusivity coefficient
e	Specific internal energy (J/Kg)
K	Thermal conductivity (W/m. K)
h	Specific enthalpy (J/Kg)
P	Pressure (Pa)
V	Volume (m^3)
T	Temperature (K)
Q	Heat (J)
m	Mass (Kg)
U	Internal energy (J)
s	Entropy (J/K)
h	Enthalpy (J/Kg)
G	Gibbs energy (J/Kg)
R	Ideal gas constant (J/mol K)
W	Work (J)
A	Availability (J)
A_w	Work availability (J)
A_q	Heat transfer availability (J)
A_{ch}	Chemical availability (J)
A_{tm}	Thermomechanical availability (J)
I	Irreversibility (J)

Abbreviations

GIE	Gross Indicated Efficiency (%)
HRR	Heat Release Rate (J/deg)
CHR	Cumulative Heat Release (J)
CA	Crank Angle
CAD	Crank Angle Degree
CA10	Crank angle of 10% heat released
CA50	Crank angle of 50% heat released
CA90	Crank angle of 90% heat released
LTC	Low-temperature combustion
SI	Spark Ignition
CI	Compression Ignition
HCCI	Homogeneous Charge-Compression Ignition
RCCI	Reactivity-Controlled Compression Ignition
CO	Carbon monoxide
CO_2	Carbon dioxide
NOx	Nitrogen oxide
HC	Hydrocarbons
EGR	Exhaust Gas Recirculation
PM	Particulate matter

IMEP	Indicated Mean Effective Pressure
BMEP	Brake Mean Effective Pressure
SOI	Start Of Injection
SOC	Start of combustion
ICE	Internal combustion engine
IVC	Inlet valve closing
EVO	Exhaust valve opening
BDC	Bottom dead center
aTDC	After the top dead center
bTDC	Before the top dead center
CFD	Computational Fluid Dynamics
DDM	Droplet distinct Model
KH-RT	Kelvin-Helmholtz-Rayleigh-Taylor
RNG	Re-Normalization Group
NTC	Nutation Time Constant
AMR	Adaptive Mesh Refinement
SMD	Sauter Mean Diameter
TKE	Turbulence kinetic energy
LHV	Lower heating value (MJ/kg)
RPM	Revolutions per minute
NG	Natural gas
BR	Brake Thermal Efficiency (%)
NHD	Nozzle Hole Diameter (μm)
NOD	Number Of Droplets
ID	Ignition Delay (deg)
EvEPI	Evaporation-Energy Performance Index (mg/ms)
EmESI	Emission-Energy Synergy Index (gr/kW.h)
ExEmBI	Exergy-Emission Balance Index (kW.h/gr)
EvEmII	Evaporation-Emission Interaction Index (kW)
ExEUI	Exergy-Energy Utilization Index (kW.h)
EmExSI	Emission-Exergy Synergy Index (gr/kW.h)
EvExPI	Evaporation-Exergy Performance Index (mg/ms)

References

[1] J. William, The Federal Government's Role in Reducing Heavy Duty Diesel Emissions, in, SAE Technical Paper, 2004.

[2] T. Kamimoto, H. Yokota, H. Kobayashi, Effect of high pressure injection on soot formation processes in a rapid compression machine to simulate diesel flames, SAE transactions, (1987) 783-791.

[3] J. Li, W. Yang, D. Zhou, Review on the management of RCCI engines, Renewable and Sustainable Energy Reviews, 69 (2017) 65-79.

[4] D. Splitter, M. Wissink, S. Kokjohn, R.D. Reitz, Effect of compression ratio and piston geometry on RCCI load limits and efficiency, in, SAE Technical Paper, 2012.

[5] A.B. Dempsey, N.R. Walker, R. Reitz, Effect of piston bowl geometry on dual fuel reactivity controlled compression ignition (RCCI) in a light-duty engine operated with gasoline/diesel and methanol/diesel, SAE International Journal of Engines, 6 (2013) 78-100.

[6] A.-H. Kakaee, A. Nasiri-Toosi, B. Partovi, A. Paykani, Effects of piston bowl geometry on combustion and emissions characteristics of a natural gas/diesel RCCI engine, Applied Thermal Engineering, 102 (2016) 1462-1472.

[7] M. Nazemian, E. Neshat, R.K. Saray, Effects of piston geometry and injection strategy on the capacity improvement of waste heat recovery from RCCI engines utilizing DOE method, Applied Thermal Engineering, 152 (2019) 52-66.

[8] K. Poorghasemi, R.K. Saray, E. Ansari, B.K. Irdmousa, M. Shahbakhti, J.D. Naber, Effect of diesel injection strategies on natural gas/diesel RCCI combustion characteristics in a light duty diesel engine, Applied energy, 199 (2017) 430-446.

[9] M. Nazemi, M. Shahbakhti, Modeling and analysis of fuel injection parameters for

A Holistic Approach to Reactivity-Controlled Compression Ignition Engine Performance: 4E Analysis (Evaporation, Energy, Emissions, Exergy) and Multidimensional Efficiency Metrics under Varying Engine Speed

combustion and performance of an RCCI engine, Applied energy, 165 (2016) 135-150.

[10] J. Benajes, S. Molina, A. García, E. Belarte, M. Vanvolsem, An investigation on RCCI combustion in a heavy duty diesel engine using in-cylinder blending of diesel and gasoline fuels, Applied Thermal Engineering, 63 (2014) 66-76.

[11] Y. Li, M. Jia, Y. Liu, M. Xie, Numerical study on the combustion and emission characteristics of a methanol/diesel reactivity controlled compression ignition (RCCI) engine, Applied energy, 106 (2013) 184-197.

[12] D.E. Nieman, A.B. Dempsey, R.D. Reitz, Heavy-duty RCCI operation using natural gas and diesel, SAE International Journal of Engines, 5 (2012) 270-285.

[13] Y. Li, M. Jia, Y. Chang, Y. Liu, M. Xie, T. Wang, L. Zhou, Parametric study and optimization of a RCCI (reactivity controlled compression ignition) engine fueled with methanol and diesel, Energy, 65 (2014) 319-332.

[14] M. Nazemian, M. Nazemian, M. Hosseini Bohloli, H. Hosseini Bohloli, M.R. HosseiniTazek, Role of Nozzle Hole Diameter in Modulating Spray Dynamics and Enhancing Combustion Performance in Reactivity-Controlled Compression Ignition Engines, Automotive Science and Engineering, 14 (2024) 4479-4502.

[15] H. Liu, X. Wang, Z. Zheng, J. Gu, H. Wang, M. Yao, Experimental and simulation investigation of the combustion characteristics and emissions using n-butanol/biodiesel dual-fuel injection on a diesel engine, Energy, 74 (2014) 741-752.

[16] C. Yu, J. Wang, W. Yu, J. Liu, D. Gao, Research on low temperature combustion of homogeneous charge induced ignition (HCII) in a light-duty diesel engine, in: Proceedings of the FISITA 2012 World Automotive Congress: Volume 1: Advanced Internal Combustion Engines (I), Springer, 2013, pp. 195-204.

[17] S. Ma, Z. Zheng, H. Liu, Q. Zhang, M. Yao, Experimental investigation of the effects of diesel injection strategy on gasoline/diesel dual-fuel combustion, Applied energy, 109 (2013) 202-212.

[18] Y. Wu, R.D. Reitz, Effects of exhaust gas recirculation and boost pressure on reactivity controlled compression ignition engine at high load operating conditions, Journal of Energy Resources Technology, 137 (2015) 032210.

[19] U. Asad, P. Divekar, M. Zheng, J. Tjong, Low temperature combustion strategies for compression ignition engines: operability limits and challenges, in, SAE Technical Paper, 2013.

[20] A. Paykani, A.-H. Kakaee, P. Rahnama, R.D. Reitz, Effects of diesel injection strategy on natural gas/diesel reactivity controlled compression ignition combustion, Energy, 90 (2015) 814-826.

[21] J. Benajes, A. Garcia, J. Monsalve-Serrano, V. Boronat, Particulates size distribution of reactivity controlled compression ignition (RCCI) on a medium-duty engine fueled with diesel and gasoline at different engine speeds, SAE International Journal of Engines, 10 (2017) 2382-2391.

[22] M. Dahodwala, S. Joshi, E. Koehler, M. Franke, D. Tomazic, Experimental and computational analysis of diesel-natural gas RCCI combustion in heavy-duty engines, in, SAE Technical Paper, 2015.

[23] R. Hanson, A. Ickes, T. Wallner, Comparison of RCCI operation with and without EGR over the full operating map of a heavy-duty diesel engine, in, SAE Technical Paper, 2016.

[24] Y. Wang, Z. Zhu, M. Yao, T. Li, W. Zhang, Z. Zheng, An investigation into the RCCI engine operation under low load and its achievable operational range at different engine speeds, Energy conversion and management, 124 (2016) 399-413.

[25] C. Rakopoulos, E. Giakoumis, Development of cumulative and availability rate balances in a multi-cylinder turbocharged indirect injection diesel engine, Energy conversion and management, 38 (1997) 347-369.

[26] C. Rakopoulos, M. Scott, D. Kyritsis, E. Giakoumis, Availability analysis of hydrogen/natural gas blends combustion in internal combustion engines, Energy, 33 (2008) 248-255.

[27] J.A. Caton, On the destruction of availability (exergy) due to combustion processes—with specific application to internal-combustion engines, Energy, 25 (2000) 1097-1117.

[28] İ. Uçkan, A. Yakın, R. Behçet, Second law analysis of an internal combustion engine for different fuels consisting of NaBH4, ethanol and methanol mixtures, International Journal of Hydrogen Energy, 49 (2024) 1257-1267.

[29] M. Proniewicz, K. Petela, A. Szlęk, G. Przybyła, E. Nadimi, Ł. Ziółkowski, T. Løvås, W. Adamczyk, Energy and Exergy Assessments of a Diesel-, Biodiesel-, and Ammonia-Fueled Compression Ignition Engine, International Journal of Energy Research, 2023 (2023) 9920670.

[30] D. Singh, A. Paul, Energy, exergy, emission, exergoeconomic, enviroeconomic, and sustainability analysis of diesel engine, fueled by waste cooking oil and waste polyethylene co-pyrolysis oil-diesel blends, Journal of Cleaner Production, 426 (2023) 139186.

[31] A. Amjad, R.K. Saray, S. Mahmoudi, A. Rahimi, Availability analysis of n-heptane and natural gas blends combustion in HCCI engines, Energy, 36 (2011) 6900-6909.

[32] H. Feng, C. Zhang, M. Wang, D. Liu, X. Yang, C.-f. Lee, Availability analysis of n-heptane/iso-octane blends during low-temperature engine combustion using a single-zone combustion model, Energy conversion and management, 84 (2014) 613-622.

[33] E. Neshat, R.K. Saray, V. Hosseini, Investigation of the effect of reformer gas on PRFs HCCI combustion based on exergy analysis, International Journal of Hydrogen Energy, 41 (2016) 4278-4295.

[34] A. Khaliq, F. Khalid, P. Sharma, I. Dincer, Energetic and exergetic analyses of a hydrogen-fuelled HCCI engine for environmentally benign operation, International Journal of Sustainable Energy, 33 (2014) 367-385.

[35] A. Khaliq, S.K. Trivedi, Second law assessment of a wet ethanol fuelled HCCI engine combined with organic Rankine cycle, (2012).

[36] A. Khaliq, S.K. Trivedi, I. Dincer, Investigation of a wet ethanol operated HCCI engine based on first and second law analyses, Applied Thermal Engineering, 31 (2011) 1621-1629.

[37] Y. Li, M. Jia, Y. Chang, S.L. Kokjohn, R.D. Reitz, Thermodynamic energy and exergy analysis of three different engine combustion regimes, Applied energy, 180 (2016) 849-858.

[38] Y. Li, M. Jia, Y. Chang, G. Xu, Comparing the exergy destruction of methanol and gasoline in reactivity controlled compression ignition (RCCI) engine, in, SAE Technical Paper, 2017.

[39] M. Mohebbi, M. Reyhanian, I. Ghofrani, A.A. Aziz, V. Hosseini, Availability analysis on combustion of n-heptane and isooctane blends in a reactivity controlled compression ignition engine, Proceedings of the Institution of Mechanical Engineers, Part D: Journal of Automobile Engineering, 232 (2018) 1501-1515.

[40] E. Neshat, M. Nazemian, R. Khoshbakhti, Effect of Start of Injection Timing on Waste Heat Recovery Capacity in a Reactivity Controlled Compression Ignition Engine,

Amirkabir Journal of Mechanical Engineering, 53 (2021) 3-16.

[41] N. Kousheshi, M. Yari, A. Paykani, A. Saberi Mehr, G.F. de la Fuente, Effect of syngas composition on the combustion and emissions characteristics of a syngas/diesel RCCI engine, Energies, 13 (2020) 212.

[42] C. Tiwari, T.N. Verma, G. Dwivedi, P. Verma, Energy-exergy analysis of diesel engine fueled with microalgae biodiesel-diesel blend, Applied Sciences, 13 (2023) 1857.

[43] F. Hamdi, S. Agrebi, M.S. Idrissi, K. Mondo, Z. Labiadh, A. Sadiki, M. Chrigui, Impact of spray cone angle on the performances of methane/diesel RCCI engine combustion under low load operating conditions, Entropy, 24 (2022) 650.

[44] M. Alipour, M. Ehghaghi, M. Mirsalim, F. Ranjbar, Energy and exergy analysis of the dual-fuel RCCI engine by ozone-assisted combustion of a lean mixture, Journal of Thermal Analysis and Calorimetry, 143 (2021) 3677-3686.

[45] X. Zhang, J. Wei, H. Liu, Y. Cai, H. Wang, M. Yao, The relationship between fuel reactivity and exergy features in combustion process, Energy, 288 (2024) 129843.

[46] B. Doğan, D. Erol, The investigation of energy and exergy analyses in compression ignition engines using diesel/biodiesel fuel blends-a review, Journal of Thermal Analysis and Calorimetry, 148 (2023) 1765-1782.

[47] S. Halis, B. Doğan, Effects of intake air temperature on energy, exergy and sustainability analyses in an RCCI engine fueled with iso-propanol and n-heptane, Energy, 284 (2023) 129050.

[48] P. Deb, A. Paul, Effect of acetylene as a low reactivity fuel on performance, combustion, exergy and emissions of an acetylene/diesel RCCI engine with variable premix ratios, Sustainable Energy & Fuels, 7 (2023) 4547-4566.

[49] B. Ma, Q. Zhan, A. Yao, C. Yao, Exergy analysis of a diesel methanol dual fuel engine with different regulatory strategies for meeting China VI emission regulations, Case Studies in Thermal Engineering, 63 (2024) 105350.

[50] M. Kumar, A. Paul, Comparative evaluation of combustion, performance, exergy and emission characteristics in hydrogen-biodiesel dual fuel engine under RCCI mode, Energy & Environment, 35 (2024) 3418-3440.

[51] H. Feng, X. Chen, L. Sun, R. Ma, X. Zhang, L. Zhu, C. Yang, The effect of methanol/diesel fuel blends with co-solvent on diesel engine combustion based on experiment and exergy analysis, Energy, 282 (2023) 128792.

[52] H. Taghavifar, A. Nemati, F.J. Salvador, J. De la Morena, 1D energy, exergy, and performance assessment of turbocharged diesel/hydrogen RCCI engine at different levels of diesel, hydrogen, compressor pressure ratio, and combustion duration, International Journal of Hydrogen Energy, 46 (2021) 22180-22194.

[53] B. Doğan, S. Halis, A. Arslan, Towards sustainable combustion: A comprehensive exergoeconomic and exergoenvironmental analysis with LCA integration for an RCCI engine, Fuel, 387 (2025) 134406.

[54] A. Asgari, M.Y. Faal, M. Yari, M. Mohebbi, R. Mahmoodi, S. Noorzadeh, Optimizing Co-generation performance of reactivity controlled compression ignition engines with solar steam reforming of methanol; a thermoeconomic, economic and exergoenvironmental analysis, International Journal of Hydrogen Energy, 94 (2024) 145-165.

[55] K. Bayramoğlu, T. Bayramoğlu, F. Polat, S. Sarıdemir, N. Alçelik, Ü. Ağbulut, Energy, exergy, and emission (3E) analysis of hydrogen-

enriched waste biodiesel-diesel fuel blends on an indirect injection dual-fuel CI engine, Energy, 314 (2025) 134124.

[56] R. Saravanan, P.N. Krishnan, M. Rengasamy, V. Manieniyan, Energy, Exergy, Entropy, Emission Factors (4E's) and Sustainability Index analyses of thermal splintering waste paraffin Oil, di-ethyl ether–diesel blends, Ain Shams Engineering Journal, 16 (2025) 103190.

[57] S. Manickam, S.K. Kasinathan, M. Gurusamy, M.M. Al-Ansari, B. Subramanian, Effect of hydrogen and diethyl ether addition on 5E attributes of compression ignition engine using papaya seed oil-diesel blend, International Journal of Hydrogen Energy, (2024).

[58] A. Rahimi, E. Fatehifar, R.K. Saray, Development of an optimized chemical kinetic mechanism for homogeneous charge compression ignition combustion of a fuel blend of n-heptane and natural gas using a genetic algorithm, Proceedings of the institution of mechanical engineers, Part D: Journal of Automobile Engineering, 224 (2010) 1141-1159.

[59] J.K. Dukowicz, A particle-fluid numerical model for liquid sprays, Journal of computational Physics, 35 (1980) 229-253.

[60] D.P. Schmidt, C.J. Rutland, A new droplet collision algorithm, Journal of computational Physics, 164 (2000) 62-80.

[61] J.C. Beale, R.D. Reitz, Modeling spray atomization with the Kelvin-Helmholtz/Rayleigh-Taylor hybrid model, Atomization and sprays, 9 (1999).

[62] Z. Han, R.D. Reitz, Turbulence modeling of internal combustion engines using RNG κ-ε models, Combustion science and technology, 106 (1995) 267-295.

[63] S.L. Post, J. Abraham, Modeling the outcome of drop–drop collisions in Diesel sprays, International Journal of Multiphase Flow, 28 (2002) 997-1019.

[64] P.J. O'Rourke, A. Amsden, A spray/wall interaction submodel for the KIVA-3 wall film model, SAE transactions, (2000) 281-298.

[65] M. Raju, M. Wang, M. Dai, W. Piggott, D. Flowers, Acceleration of detailed chemical kinetics using multi-zone modeling for CFD in internal combustion engine simulations, in, SAE Technical Paper, 2012.

[66] M. Nazemi, Modeling and analysis of reactivity controlled compression ignition (RCCI) combustion, in, Michigan Technological University, 2015.

[67] K. Poorghasemi, R. Khoshbakhti Saray, E. Ansari, S.M. Mousavi, A. Zehni, Statistical analysis on the effect of premixed ratio, EGR, and diesel fuel injection parameters on the performance and emissions of a NG/Diesel RCCI engine using a DOE method, Proceedings of the institution of mechanical engineers, Part D: Journal of Automobile Engineering, 236 (2022) 460-473.

[68] P. Rahnama, A. Paykani, V. Bordbar, R.D. Reitz, A numerical study of the effects of reformer gas composition on the combustion and emission characteristics of a natural gas/diesel RCCI engine enriched with reformer gas, Fuel, 209 (2017) 742-753.

[69] P. Rahnama, A. Paykani, R.D. Reitz, A numerical study of the effects of using hydrogen, reformer gas and nitrogen on combustion, emissions and load limits of a heavy duty natural gas/diesel RCCI engine, Applied Energy, 193 (2017) 182-198.

[70] T.Y. Motlagh, L.N. Azadani, K. Yazdani, Multi-objective optimization of diesel injection parameters in a natural gas/diesel reactivity controlled compression ignition engine, Applied energy, 279 (2020) 115746.

[71] E. Ansari, T. Menucci, M. Shahbakhti, J. Naber, Experimental investigation into effects of

high reactive fuel on combustion and emission characteristics of the Diesel-Natural gas Reactivity Controlled Compression Ignition engine, Applied energy, 239 (2019) 948-956.

[72] K.O.P. Bjørgen, D.R. Emberson, T. Løvås, Combustion of liquid ammonia and diesel in a compression ignition engine operated in high-pressure dual fuel mode, Fuel, 360 (2024) 130269.

[73] J. Li, W.M. Yang, T.N. Goh, H. An, A. Maghbouli, Study on RCCI (reactivity controlled compression ignition) engine by means of statistical experimental design, Energy, 78 (2014) 777-787.

[74] J. Shu, J. Fu, W. Yang, J. Huang, T. He, J. Liu, Experimental and computational study on the effects of exhaust gas recirculation on thermodynamics, combustion and emission characteristics of a diesel pilot ignition natural gas engine, Sustainable Energy & Fuels, 8 (2024) 3630-3644.

[75] Z. Lin, S. Liu, Y. Qi, Q. Chen, Z. Wang, Experimental study on the performance of a high compression ratio SI engine using alcohol/ammonia fuel, Energy, 289 (2024) 129998.

[76] S. Jafarmadar, P. Nemati, Exergy analysis of diesel/biodiesel combustion in a homogenous charge compression ignition (HCCI) engine using three-dimensional model, Renewable energy, 99 (2016) 514-523.

[77] C.D. Rakopoulos, D.C. Kyritsis, Comparative second-law analysis of internal combustion engine operation for methane, methanol, and dodecane fuels, Energy, 26 (2001) 705-722.

[78] M.A.S. Al-Baghdadi, Effect of compression ratio, equivalence ratio and engine speed on the performance and emission characteristics of a spark ignition engine using hydrogen as a fuel, Renewable energy, 29 (2004) 2245-2260.

[79] A.-H. Kakaee, P. Jafari, A. Paykani, Numerical study of natural gas/diesel reactivity controlled compression ignition combustion with large eddy simulation and reynolds-averaged navier–stokes model, Fluids, 3 (2018) 24.

[80] H.D. Disassa, V.R. Ancha, R.B. Nallamothu, B.A. Zeru, Experimental study on the effect of speed and port-injected fuel blend ratio on a reactivity-control compression ignition (RCCI) engine performance, Energy conversion and management: X, 20 (2023) 100448.

[81] A. Zarenejad Ashkezari, M.R. Hadavi, Modeling and Prediction of Fuel Consumption and Emissions of Direct Injection Diesel Engines using Artificial Neural Network by Applying Control Parameters of Engine Speed, Fuel Mass and Inlet Air Temperature, Journal of Solid and Fluid Mechanics, 10 (2020) 237-251.